Damage-plastic model for concrete failure

Peter Grassl [a,*], Milan Jirásek [b]

[a] *Department of Civil Engineering, University of Glasgow, Glasgow G12 8LT, United Kingdom*
[b] *Department of Mechanics, Faculty of Civil Engineering, Czech Technical University in Prague, Czech Republic*

Abstract

The present paper deals with the combination of plasticity and damage applied to modeling of concrete failure. First, the local uniqueness conditions of two types of combinations of stress-based plasticity and strain-driven scalar damage are studied. Then a triaxial damage-plastic model for the failure of concrete is presented. The plasticity part is based on the effective stress and the damage model is driven by the plastic strain. The implementation of the model in the form of a fully implicit integration scheme is discussed and the corresponding algorithmic stiffness matrix is derived. The constitutive response is compared to a wide range of experimental results. Finally, the model is applied to the structural analysis of reinforced concrete columns. A regularized version of this model with weighted spatial averaging of the damage-driving variable is published in a separate paper.
© 2006 Elsevier Ltd. All rights reserved.

Keywords: Plasticity; Damage mechanics; Concrete; Failure

1. Introduction

Typical failure modes of concrete are cracking in tension and crushing in compression. The failure process is characterized by irreversible deformations and degradation of the material stiffness, which leads in tension and unconfined or low-confined compression to strain softening, i.e. decreasing stress under increasing strain. In low-confined compression, softening is accompanied by extensive inelastic volumetric expansion. In highly confined compression, on the other hand, the stiffness degradation and the inelastic volume expansion are significantly reduced.

One group of constitutive models suitable for the description of these complex phenomena is based on a combination of the flow theory of plasticity with damage mechanics. Plasticity models alone, for instance those proposed by Chen and Chen (1975), Dragon and Mróz (1979), Lin et al. (1987), Pramono and Willam (1989), Etse and Willam (1994), Pekau and Zhang (1994), Lade and Kim (1995), Menétrey and Willam (1995), Feenstra and de Borst (1996), Kang (1997), or Grassl et al. (2002), are unable to capture the stiffness

---

degradation observed in experiments. Damage models, on the other hand, are not suitable for description of irreversible deformations and of inelastic volumetric expansion in compression; see for instance Mazars (1984).

Combinations of plasticity and damage usually consider plasticity with isotropic hardening and enrich it by either isotropic or anisotropic damage. Anisotropic damage models for brittle materials, such as concrete, are often complex and a combination with plasticity and application to structural analysis is not straightforward; see Carol et al. (2001) and Hansen et al. (2001). Isotropic damage, on the other hand, is widely used (Gatuingt and Pijaudier-Cabot, 2002; Bourgeois et al., 2003; Krätzig and Polling, 2004; Salari et al., 2004; Jason et al., in press) and different types of combinations with plasticity models have been proposed in the literature. One group of models relies on stress-based plasticity formulated in the effective stress space; see for instance Ju (1989), Lee and Fenves (1998) and Jason et al. (2004). Another group of models is based on plasticity formulated in the nominal stress space; see for instance Lubliner et al. (1989), Imran and Pantazopoulou (2001) and Ananiev and Ožbolt (2004). Here, effective stress is meant as the average micro-level stress acting in the undamaged material between defects, defined as force divided by the undamaged part of the area, while nominal stress is meant as the macro-level stress and is defined as force divided by the total area.

In the present paper we study the local uniqueness conditions for the two different groups of models, i.e., we determine whether any prescribed strain history generates a unique response in terms of stress and internal variables. Models that violate the uniqueness conditions do not possess a unique solution for certain histories and are therefore unsuitable for structural analysis. This type of local uniqueness study is well known from multi-surface plasticity; see for instance Chapter 20 in Jirásek and Bažant (2002). For combinations of damage and plasticity, however, the issue of local uniqueness has not received much attention in the literature, even though the conditions sometimes turn out to be more restrictive than for multi-surface plasticity.

Furthermore, we present a new damage-plastic approach to modeling concrete failure under general triaxial stress covering tension, shear and multiaxial compression with different levels of confinement. We discuss the implementation of the model and compare the model response to experimental results in the literature.

Of course, a local constitutive model with nonassociated flow and softening cannot provide an objective description of localized failure modes and needs to be adjusted or regularized. As a first remedy, we use a simple engineering approach with adjustment of the damage law (which controls softening) according to the size of the finite element, in the spirit of the traditional crack-band theory (Bažant and Oh, 1983). However, such an approach is not fully reliable in situations when localized failure patterns coexist with diffuse ones. A more sophisticated remedy is provided by a regularized formulation based on weighted spatial averaging of the damage-driving variable, which is presented in detail in a separate publication (Grassl and Jirásek, 2006).

2. Combinations of plasticity and damage

This section compares and evaluates two types of models combining stress-based plasticity with strain-based scalar damage. The analysis is focused on local uniqueness, i.e., on the question whether the response in terms of stress and internal variables is unique for any prescribed strain history.

The two groups, namely models with the plastic part written in terms of the effective stress (i.e., in the undamaged space) and those with the plasticity part written in terms of the nominal stress (in the damaged space), are studied separately. The former includes mainly formulations with focus on the combination of irreversible strains and stiffness degradation, whereas the latter comprises approaches for which the response in different domains of the stress space is described separately by the different components, for instance tensile failure by the damage part and compressive failure by the plastic part.

The stress–strain relation for all such models is

$$\boldsymbol{\sigma} = (1 - \omega)\bar{\boldsymbol{\sigma}} = (1 - \omega)\mathbf{D}_e : (\boldsymbol{\varepsilon} - \boldsymbol{\varepsilon}_p) \tag{1}$$

where ω is a scalar describing the amount of isotropic damage, $\mathbf{D}_e$ is the elastic stiffness, $\boldsymbol{\varepsilon}$ is the total strain, $\boldsymbol{\varepsilon}_p$ is the plastic strain, $\bar{\boldsymbol{\sigma}}$ is the effective stress and $\boldsymbol{\sigma}$ is the nominal stress. The evolution equations for internal variables such as ω and $\boldsymbol{\varepsilon}_p$ depend on the specific formulation; they are discussed in the subsequent sections.

2.1. Plasticity model based on effective stress

The first group of models combines plasticity based on the effective stress $\bar{\boldsymbol{\sigma}}$ with damage driven by the total strain or by the plastic strain. The plasticity model is described by the yield function, the flow rule, the evolution law for the hardening variable and the loading–unloading conditions:

$$f_p(\bar{\boldsymbol{\sigma}}, \kappa_p) = \tilde{\sigma}(\bar{\boldsymbol{\sigma}}) - \sigma_Y(\kappa_p) \tag{2}$$

$$\dot{\boldsymbol{\varepsilon}}_p = \dot{\lambda} \frac{\partial g_p}{\partial \bar{\boldsymbol{\sigma}}}(\bar{\boldsymbol{\sigma}}, \kappa_p) \tag{3}$$

$$\dot{\kappa}_p = \dot{\lambda} k_p(\bar{\boldsymbol{\sigma}}, \kappa_p) \tag{4}$$

$$f_p \leqslant 0, \quad \dot{\lambda} \geqslant 0, \quad \dot{\lambda} f_p = 0 \tag{5}$$

Here, f_p is the yield function, κ_p is the plastic hardening variable, $\tilde{\sigma}$ is the equivalent stress, σ_Y is the yield stress, λ is the plastic multiplier, g_p is the plastic potential, and k_p is a function relating the rate of the hardening variable to the rate of the plastic multiplier. Superimposed dot denotes derivative with respect to time, but the models considered here are rate-independent and the rates can also be interpreted as infinitesimal increments.

The damage model is described by the damage loading function, the evolution law for the damage variable, and the loading–unloading conditions:

$$f_d(\boldsymbol{\varepsilon}, \boldsymbol{\varepsilon}_p, \kappa_d) = \tilde{\varepsilon}(\boldsymbol{\varepsilon}, \boldsymbol{\varepsilon}_p) - \kappa_d \tag{6}$$

$$\omega = g_d(\kappa_d) \tag{7}$$

$$f_d \leqslant 0, \quad \dot{\kappa}_d \geqslant 0, \quad \dot{\kappa}_d f_d = 0 \tag{8}$$

Here, f_d is the damage loading function, $\tilde{\varepsilon}$ is the equivalent strain, κ_d is the damage-driving variable and g_d is the damage function.

Let us first elucidate the notion of local uniqueness. To keep the presentation simple, we look only at the plastic part of the model. If the current value of the yield function f_p is negative, plastic flow cannot occur because the third condition in (5) implies that $\dot{\lambda} = 0$. On the other hand, if $f_p = 0$, the material can either exhibit plastic flow characterized by $\dot{\lambda} > 0$, or unload elastically with $\dot{\lambda} = 0$. In the former case, the yield function remains equal to zero and so its rate vanishes (this is the so-called consistency condition), while in the latter case the yield function must not increase and its rate is thus nonpositive. This means that if the current state is plastic, the rates of the yield function and of the plastic multiplier must satisfy conditions

$$\dot{f}_p \leqslant 0, \quad \dot{\lambda} \geqslant 0, \quad \dot{\lambda} \dot{f}_p = 0 \tag{9}$$

that are formally similar to (5) but the value of the yield function is replaced by its rate. Differentiating (2) with respect to time and exploiting the rate form of the effective stress–strain law, $\dot{\bar{\boldsymbol{\sigma}}} = \mathbf{D}_e : (\dot{\boldsymbol{\varepsilon}} - \dot{\boldsymbol{\varepsilon}}_p)$, and the evolution equations (3) and (4), we can express

$$\dot{f}_p = \frac{\partial f_p}{\partial \bar{\boldsymbol{\sigma}}} : \dot{\bar{\boldsymbol{\sigma}}} + \frac{\partial f_p}{\partial \kappa_p} \dot{\kappa}_p = \frac{\partial f_p}{\partial \bar{\boldsymbol{\sigma}}} : \mathbf{D}_e : \dot{\boldsymbol{\varepsilon}} - \dot{\lambda} \left(\frac{\partial f_p}{\partial \bar{\boldsymbol{\sigma}}} : \mathbf{D}_e : \frac{\partial g_p}{\partial \bar{\boldsymbol{\sigma}}} + H_p k_p \right) \tag{10}$$

where

$$H_p = -\frac{\partial f_p}{\partial \kappa_p} = \frac{d\sigma_Y}{d\kappa_p} \tag{11}$$

is the plastic modulus, positive for hardening and negative for softening. Substituting (10) into (9), we obtain the so-called linear complementarity problem (LCP) for the unknown rate of the plastic multiplier, $\dot{\lambda}$. It is easy to show that if the expression in parentheses in (10) is positive, the LCP has a unique solution for any given strain rate $\dot{\boldsymbol{\varepsilon}}$. On the other hand, if that expression is negative, no solution exists for those strain rates that render the expression $\frac{\partial f_p}{\partial \bar{\boldsymbol{\sigma}}} : \mathbf{D}_e : \dot{\boldsymbol{\varepsilon}}$ positive, and two solutions exist for strain rates that render this expression negative. A nonunique situation arises also when the expression in parentheses in (10) is zero. This means that the condition of local uniqueness reads

$$\frac{\partial f_{\mathrm{p}}}{\partial \overline{\boldsymbol{\sigma}}} : \mathbf{D}_{\mathrm{e}} : \frac{\partial g_{\mathrm{p}}}{\partial \overline{\boldsymbol{\sigma}}} + H_{\mathrm{p}} k_{\mathrm{p}} > 0 \tag{12}$$

This condition should be satisfied for all possible states of the material. If this is not the case, there exist certain strain histories for which the corresponding stress history is not uniquely determined by the model equations, and at some stage of analysis the stress-return algorithm (evaluation of the stress increment corresponding to the given strain increment) may diverge.

We will now extend the analysis of local uniqueness to the combined damage-plastic model, considering a state satisfying both conditions $f_{\mathrm{p}} = 0$ and $f_{\mathrm{d}} = 0$. The subsequent evolution may involve plastic yielding, or damage growth, or both of these dissipative mechanisms, or neither of them. The rate problem analogous to (9) can be written in matrix form as

$$\dot{\mathbf{f}} \leqslant \mathbf{0}, \quad \dot{\boldsymbol{\lambda}} \geqslant \mathbf{0}, \quad \dot{\boldsymbol{\lambda}}^{\mathrm{T}} \dot{\mathbf{f}} = 0 \tag{13}$$

where

$$\dot{\mathbf{f}} = \left\{ \begin{array}{c} \dot{f}_{\mathrm{p}} \\ \dot{f}_{\mathrm{d}} \end{array} \right\} \tag{14}$$

and

$$\dot{\boldsymbol{\lambda}} = \left\{ \begin{array}{c} \dot{\lambda} \\ \dot{\kappa}_{\mathrm{d}} \end{array} \right\} \tag{15}$$

The rate of the yield function is expressed according to (10), and the rate of the damage loading function is expressed as

$$\dot{f}_{\mathrm{d}} = \frac{\partial f_{\mathrm{d}}}{\partial \boldsymbol{\varepsilon}} : \dot{\boldsymbol{\varepsilon}} + \frac{\partial f_{\mathrm{d}}}{\partial \boldsymbol{\varepsilon}_{\mathrm{p}}} : \dot{\boldsymbol{\varepsilon}}_{\mathrm{p}} + \frac{\partial f_{\mathrm{d}}}{\partial \kappa_{\mathrm{d}}} \dot{\kappa}_{\mathrm{d}} = \frac{\partial f_{\mathrm{d}}}{\partial \boldsymbol{\varepsilon}} : \dot{\boldsymbol{\varepsilon}} + \dot{\lambda} \frac{\partial f_{\mathrm{d}}}{\partial \boldsymbol{\varepsilon}_{\mathrm{p}}} : \frac{\partial g_{\mathrm{p}}}{\partial \overline{\boldsymbol{\sigma}}} + \frac{\partial f_{\mathrm{d}}}{\partial \kappa_{\mathrm{d}}} \dot{\kappa}_{\mathrm{d}} \tag{16}$$

and so we can write

$$\dot{\mathbf{f}} = \mathbf{b} - \mathbf{A} \dot{\boldsymbol{\lambda}} \tag{17}$$

with

$$\mathbf{A} = \begin{pmatrix} \dfrac{\partial f_{\mathrm{p}}}{\partial \overline{\boldsymbol{\sigma}}} : \mathbf{D}_{\mathrm{e}} : \dfrac{\partial g_{\mathrm{p}}}{\partial \overline{\boldsymbol{\sigma}}} + H_{\mathrm{p}} k_{\mathrm{p}} & 0 \\[2ex] -\dfrac{\partial f_{\mathrm{d}}}{\partial \boldsymbol{\varepsilon}_{\mathrm{p}}} : \dfrac{\partial g_{\mathrm{p}}}{\partial \overline{\boldsymbol{\sigma}}} & -\dfrac{\partial f_{\mathrm{d}}}{\partial \kappa_{\mathrm{d}}} \end{pmatrix} \tag{18}$$

and

$$\mathbf{b} = \left\{ \begin{array}{c} \dfrac{\partial f_{\mathrm{p}}}{\partial \overline{\boldsymbol{\sigma}}} : \mathbf{D}_{\mathrm{e}} : \dot{\boldsymbol{\varepsilon}} \\[2ex] \dfrac{\partial f_{\mathrm{d}}}{\partial \boldsymbol{\varepsilon}} : \dot{\boldsymbol{\varepsilon}} \end{array} \right\} \tag{19}$$

Substituting (17) into (13) we obtain the LCP

$$\mathbf{A} \dot{\boldsymbol{\lambda}} - \mathbf{b} \geqslant \mathbf{0}, \quad \dot{\boldsymbol{\lambda}} \geqslant \mathbf{0}, \quad \dot{\boldsymbol{\lambda}}^{\mathrm{T}} (\mathbf{A} \dot{\boldsymbol{\lambda}} - \mathbf{b}) = 0 \tag{20}$$

Note that if the current state and the strain rate are given, then $\mathbf{A}$ and $\mathbf{b}$ are known and the unknowns to be determined are the components of $\dot{\boldsymbol{\lambda}}$. It is known from optimization theory that an LCP in the form (20) has exactly one solution $\dot{\boldsymbol{\lambda}}$ for any vector $\mathbf{b}$ if and only if all the principal minors of matrix $\mathbf{A}$ are positive; see for instance Cottle et al. (1992). This results in the following conditions for the components of matrix $\mathbf{A}$:

$$A_{11} > 0, \quad A_{22} > 0, \quad A_{11} A_{22} - A_{21} A_{12} > 0 \tag{21}$$

Since in our particular case $A_{12} = 0$, the third condition follows from the first two, and it is sufficient to verify that

$$\frac{\partial f_{\mathrm{p}}}{\partial \bar{\boldsymbol{\sigma}}} : \mathbf{D}_{\mathrm{e}} : \frac{\partial g_{\mathrm{p}}}{\partial \bar{\boldsymbol{\sigma}}} + H_{\mathrm{p}} k_{\mathrm{p}} > 0 \tag{22}$$

$$-\frac{\partial f_{\mathrm{d}}}{\partial \kappa_{\mathrm{d}}} > 0 \tag{23}$$

The first condition (22) is independent of the damage part and has exactly the same form (12) as for the plasticity model alone. If the damage loading function has the assumed form (6), the second condition (23) is automatically satisfied because $\frac{\partial f_{\mathrm{d}}}{\partial \kappa_{\mathrm{d}}} = -1$.

In conclusion, the present type of combination does not imply any further restrictions on the specific form of the plastic and damage parts of the model. The damage part can depend on both the total strain and the plastic strain. Furthermore, both parts can exhibit softening, but the softening plastic modulus must not drop below a critical value, which is the same as for the pure plastic model.

2.2. Plasticity model based on nominal stress

The second group of models comprises combinations of plasticity based on the nominal stress with damage driven by the total or the plastic strain, or both. The damage part is the same as defined in (6)–(8). The plastic part, however, is different since now it is based on the nominal stress $\boldsymbol{\sigma}$, i.e., the basic equations are written as

$$f_{\mathrm{p}}(\boldsymbol{\sigma}, \kappa_{\mathrm{p}}) = \tilde{\sigma}(\boldsymbol{\sigma}) - \sigma_{\mathrm{Y}}(\kappa_{\mathrm{p}}) \tag{24}$$

$$\dot{\boldsymbol{\varepsilon}}_{\mathrm{p}} = \dot{\lambda} \frac{\partial g_{\mathrm{p}}}{\partial \boldsymbol{\sigma}} \tag{25}$$

$$\dot{\kappa}_{\mathrm{p}} = \dot{\lambda} k_{\mathrm{p}}(\boldsymbol{\sigma}, \kappa_{\mathrm{p}}) \tag{26}$$

The loading–unloading conditions keep the same format (5) as before.

Repeating the steps from the preceding section, we express the rate of the yield function by differentiating (24) with respect to time and exploiting the rate form of the stress–strain law (1) and the evolution equations (25) and (26):

$$\dot{f}_{\mathrm{p}} = \frac{\partial f_{\mathrm{p}}}{\partial \boldsymbol{\sigma}} : \dot{\boldsymbol{\sigma}} + \frac{\partial f_{\mathrm{p}}}{\partial \kappa_{\mathrm{p}}} \dot{\kappa}_{\mathrm{p}} = (1 - \omega) \frac{\partial f_{\mathrm{p}}}{\partial \boldsymbol{\sigma}} : \mathbf{D}_{\mathrm{e}} : \dot{\boldsymbol{\varepsilon}} - \dot{\lambda} \left[(1 - \omega) \frac{\partial f_{\mathrm{p}}}{\partial \boldsymbol{\sigma}} : \mathbf{D}_{\mathrm{e}} : \frac{\partial g_{\mathrm{p}}}{\partial \boldsymbol{\sigma}} + H_{\mathrm{p}} k_{\mathrm{p}} \right] - \dot{\kappa}_{\mathrm{d}} \frac{\mathrm{d} g_{\mathrm{d}}}{\mathrm{d} \kappa_{\mathrm{d}}} \frac{\partial f_{\mathrm{p}}}{\partial \boldsymbol{\sigma}} : \bar{\boldsymbol{\sigma}} \tag{27}$$

The rate of the damage loading function is given by (16) with $\partial g_{\mathrm{p}}/\partial \bar{\boldsymbol{\sigma}}$ replaced by $\partial g_{\mathrm{p}}/\partial \boldsymbol{\sigma}$. The resulting LCP has the general form (20) but matrix $\mathbf{A}$ is now given by

$$\mathbf{A} = \begin{pmatrix} (1 - \omega) \dfrac{\partial f_{\mathrm{p}}}{\partial \boldsymbol{\sigma}} : \mathbf{D}_{\mathrm{e}} : \dfrac{\partial g_{\mathrm{p}}}{\partial \boldsymbol{\sigma}} + H_{\mathrm{p}} k_{\mathrm{p}} & \dfrac{\mathrm{d} g_{\mathrm{d}}}{\mathrm{d} \kappa_{\mathrm{d}}} \dfrac{\partial f_{\mathrm{p}}}{\partial \boldsymbol{\sigma}} : \bar{\boldsymbol{\sigma}} \\ -\dfrac{\partial f_{\mathrm{d}}}{\partial \boldsymbol{\varepsilon}_{\mathrm{p}}} : \dfrac{\partial g_{\mathrm{p}}}{\partial \boldsymbol{\sigma}} & 1 \end{pmatrix} \tag{28}$$

Note that we have considered the damage loading function in the form (6), and so $\frac{\partial f_{\mathrm{d}}}{\partial \kappa_{\mathrm{d}}} = -1$. The three conditions of uniqueness (21) are now written as

$$(1 - \omega) \frac{\partial f_{\mathrm{p}}}{\partial \boldsymbol{\sigma}} : \mathbf{D}_{\mathrm{e}} : \frac{\partial g_{\mathrm{p}}}{\partial \boldsymbol{\sigma}} + H_{\mathrm{p}} k_{\mathrm{p}} > 0 \tag{29}$$

$$1 > 0 \tag{30}$$

$$(1 - \omega) \frac{\partial f_{\mathrm{p}}}{\partial \boldsymbol{\sigma}} : \mathbf{D}_{\mathrm{e}} : \frac{\partial g_{\mathrm{p}}}{\partial \boldsymbol{\sigma}} + H_{\mathrm{p}} k_{\mathrm{p}} > -\frac{\partial f_{\mathrm{d}}}{\partial \boldsymbol{\varepsilon}_{\mathrm{p}}} : \frac{\partial g_{\mathrm{p}}}{\partial \boldsymbol{\sigma}} \left(\frac{\mathrm{d} g_{\mathrm{d}}}{\mathrm{d} \kappa_{\mathrm{d}}} \frac{\partial f_{\mathrm{p}}}{\partial \boldsymbol{\sigma}} : \bar{\boldsymbol{\sigma}} \right) \tag{31}$$

The first condition (29) is in the undamaged state ($\omega = 0$) identical to (22). However, as damage grows, the first term is reduced and finally disappears. For the fully damaged state ($\omega = 1$) the condition is fulfilled only if

$$H_{\mathrm{p}} k_{\mathrm{p}} > 0 \tag{32}$$

Since the scaling factor k_p is positive, condition (32) means that the plastic modulus must be positive as well, i.e., plastic softening is excluded. The second condition (30) is always satisfied for damage loading functions in the form (6). The third condition (31) can become even more restrictive than the first one, as will be illustrated by an example.

Consider combination of Drucker–Prager plasticity with isotropic damage using a Rankine-type loading function. The yield function and the plastic potential of the Drucker–Prager plasticity model are defined as

$$f_p(\boldsymbol{\sigma}, \kappa_p) = c_\phi I_1(\boldsymbol{\sigma}) + \sqrt{J_2(\boldsymbol{\sigma})} - \sigma_Y(\kappa_p) \tag{33}$$

$$g_p(\boldsymbol{\sigma}) = c_\psi I_1(\boldsymbol{\sigma}) + \sqrt{J_2(\boldsymbol{\sigma})} \tag{34}$$

where $I_1 = \boldsymbol{\sigma} : \boldsymbol{\delta}$ is the trace of the stress tensor, $\boldsymbol{\delta}$ is the Kronecker delta, $J_2 = \mathbf{s} : \mathbf{s}/2$ is the second invariant of the deviatoric stress $\mathbf{s} = \boldsymbol{\sigma} - \boldsymbol{\delta} I_1/3$, c_ϕ is the friction coefficient, c_ψ is the dilation coefficient and σ_Y is the yield stress in shear.

The loading function of the Rankine damage model has the form (6) with the equivalent strain $\tilde{\varepsilon}$ given by

$$\tilde{\varepsilon}(\boldsymbol{\varepsilon}, \boldsymbol{\varepsilon}_p) = \frac{1}{E} \max_{I=1,2,3} \langle \bar{\sigma}_I(\boldsymbol{\varepsilon}, \boldsymbol{\varepsilon}_p) \rangle \tag{35}$$

where E is Young's modulus, $\langle \cdot \rangle$ are the McAuley brackets (positive-part operator), and $\bar{\sigma}_I$ is the Ith principal value of the effective stress tensor $\bar{\boldsymbol{\sigma}} = \mathbf{D}_e : (\boldsymbol{\varepsilon} - \boldsymbol{\varepsilon}_p)$. Damage is linked to variable κ_d through (7) with

$$g_d(\kappa_d) = \begin{cases} 0 & \text{if } \kappa_d \leqslant \varepsilon_0 \\ 1 - \dfrac{\varepsilon_0}{\kappa_d} \exp\left(-\dfrac{\kappa_d - \varepsilon_0}{\varepsilon_f - \varepsilon_0}\right) & \text{if } \kappa_d \geqslant \varepsilon_0 \end{cases} \tag{36}$$

where ε_0 is the strain at peak stress under uniaxial tension and ε_f is a parameter that controls the slope of the exponential softening curve.

The equivalent strain in (35) depends on the elastic strain $\boldsymbol{\varepsilon}_e = \boldsymbol{\varepsilon} - \boldsymbol{\varepsilon}_p$, so that (16) is reformulated as

$$\dot{f}_d = \frac{\partial f_d}{\partial \boldsymbol{\varepsilon}_e} : \dot{\boldsymbol{\varepsilon}}_e + \frac{\partial f_d}{\partial \kappa_d} \dot{\kappa}_d = \frac{\partial \tilde{\varepsilon}}{\partial \boldsymbol{\varepsilon}_e} : \left(\dot{\boldsymbol{\varepsilon}} - \dot{\lambda} \frac{\partial g_p}{\partial \boldsymbol{\sigma}} \right) - \dot{\kappa}_d \tag{37}$$

Thus, condition (31) reads

$$(1 - \omega) \frac{\partial f_p}{\partial \boldsymbol{\sigma}} : \mathbf{D}_e : \frac{\partial g_p}{\partial \boldsymbol{\sigma}} + H_p k_p > \frac{\partial \tilde{\varepsilon}}{\partial \boldsymbol{\varepsilon}_e} : \frac{\partial g_p}{\partial \boldsymbol{\sigma}} \left(\frac{dg_d}{d\kappa_d} \frac{\partial f_p}{\partial \boldsymbol{\sigma}} : \bar{\boldsymbol{\sigma}} \right) \tag{38}$$

Substituting the derivatives of the Drucker–Prager yield function (33), of plastic potential (34), of expression (35) for the equivalent strain and of the damage law (36) into (38) gives, after some algebraic manipulations, the uniqueness condition

$$(1 - \omega) E \left(\frac{3 c_\phi c_\psi}{1 - 2v} + \frac{1}{2(1 + v)} \right) + H_p k_p > \left(\frac{1}{\kappa_d} + \frac{1}{\varepsilon_f - \varepsilon_0} \right) \left(\frac{c_\psi}{(1 - 2v)} + \frac{s_1}{2(1 + v)\sqrt{J_2}} \right) \sigma_Y(\kappa_p) \tag{39}$$

where v is Poisson's ratio and s_1 is the maximum principal deviatoric stress.

To gain more insight, we select specific values of the model parameters. The friction coefficient is chosen as $c_\phi = 0.07$, which corresponds to the ratio between biaxial and uniaxial compressive strengths $\bar{f}_b/\bar{f}_c = 1.16$; the corresponding initial value of σ_Y is $\sigma_0 = (\sqrt{3}/3 - c_\phi)\bar{f}_c = 0.50735\bar{f}_c$. The dilation coefficient is set to $c_\psi = 0.05$, which results in a realistic prediction of volumetric expansion under uniaxial compression. The ratio between the compressive and tensile strengths is taken as $\bar{f}_c/\bar{f}_t = 10$, and the elastic limit strain is $\varepsilon_0 = \bar{f}_t/E$.

Consider the stress state at the intersection of the damage and plastic surfaces under plane stress; cf. Fig. 1. The positive principal stress is $\sigma_1 = \bar{f}_t$, the out-of-plane principal stress is $\sigma_3 = 0$, and the negative principal stress $\sigma_2 = -0.925\bar{f}_c = -9.25\bar{f}_t$ can be computed from the yield condition. From principal stresses we can evaluate the stress invariants $I_1 = -0.825\bar{f}_c$ and $J_2 = 0.3194\bar{f}_c^2$. At the elastic limit, the initial values of damage, damage hardening variables and yield stress are $\omega = 0$, $\kappa_d = \varepsilon_0 = \bar{f}_t/E$ and $\sigma_Y(0) = \sigma_0 = 0.50735\bar{f}_c = 5.0735\bar{f}_t$. Substituting all this into (39), we obtain the following restriction on the generalized plastic hardening modulus:
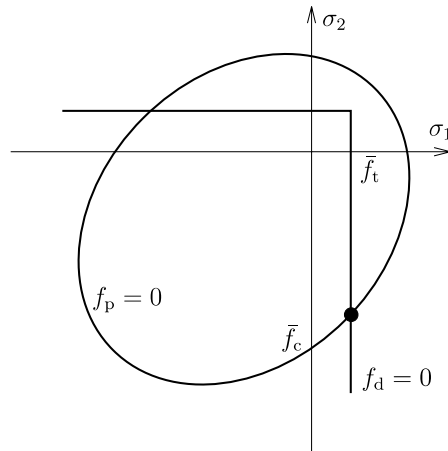
Fig. 1. Schematic drawing of the yield surface of the plasticity model and the loading function of the damage in the principal stress space at the onset of damage ($\omega = 0$).

$$H_{p}k_{p} > \left(\frac{1.8257}{1 - \varepsilon_0/\varepsilon_f} - 0.4342 \right) E > 1.3915E \tag{40}$$

Parameter ε_f controlling the slope of the tensile softening diagram depends on the fracture energy and on the size of finite elements, but even in the most favorable case of very large value of ε_f (corresponding to very small elements), the generalized plastic hardening modulus must be larger than Young's modulus, otherwise the uniqueness condition is violated. Hence the local uniqueness is guaranteed only with a strong amount of hardening in the plasticity model. This is not acceptable for modeling concrete in uniaxial and weakly confined compression.

As mentioned before, if the damage loading function is independent of the plastic strain, then component A_{21} in (28) vanishes and condition (31) is equivalent to (29). Damage driven exclusively by the total strain, however, is not appropriate for combined damage-plastic models for concrete. If the material is loaded in compression and considerable negative plastic strains develop, upon subsequent load reversal (removal of the compressive stress followed by tensile loading) damage must start already when the total strain is still negative but the stress (proportional to the elastic strain) exceeds the tensile strength (Fig. 2). Thus, damage loading functions dependent of the total strain only would produce spurious effects upon load reversal.
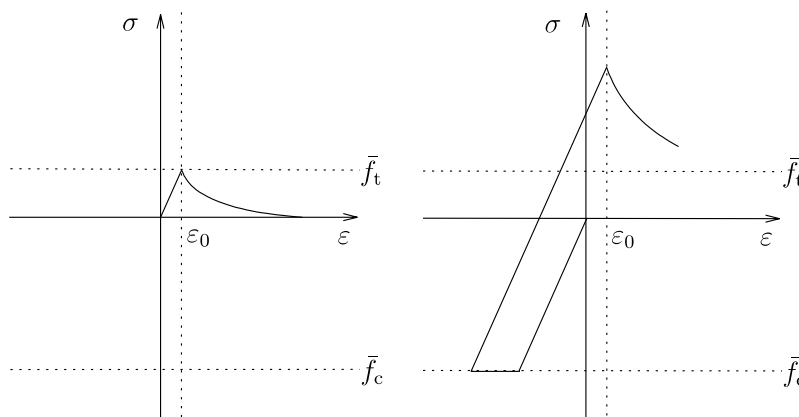

Fig. 2. Typical stress–strain response in uniaxial tension of a damage model driven by the total strain without and with preceding compressive loading.

2.3. Choice of suitable framework

In the preceding sections, the local uniqueness conditions for two different combinations of stress-based plasticity and strain-driven damage were studied. For the first group of models, the plastic part is based on the effective stress, while for the second group it is based on the nominal stress. The damage evolution may depend on the total strain as well as on the plastic strain. For the first group, the combination of plasticity and damage does not result in further restriction on the model parameters. For the second group, the plastic part must exhibit strong hardening to fulfill the local uniqueness conditions. This is a severe restriction, since for this combination the response in compression would be modeled by hardening plasticity alone, whereas experimental results show softening for uniaxial and low-confined compression. Consequently, in the proposed damage-plastic model for concrete, to be presented in the next section, the plastic part is based on the effective stress.

3. Damage-plastic model for concrete failure

In the present section a triaxial damage-plastic model for concrete failure is developed. The plastic part of the model is based on the effective stress and is defined by the yield function, the flow rule, the evolution law for the hardening variable, and the loading–unloading conditions as stated in (2)–(5). The damage model is based on the plastic strain and consists of the damage loading function, the damage law, and the loading–unloading conditions as stated in (6)–(8). In the following sections, the basic components of the plastic and damage parts of the model are specified in detail.

3.1. Components of the plasticity model

The plasticity model is formulated in a three-dimensional framework with a pressure-sensitive yield surface, hardening and nonassociated flow. The main components are the yield condition, the hardening law, the evolution law for the hardening variable and the flow rule.

3.1.1. Yield surface

The yield surface is described in terms of the cylindrical coordinates in the principal effective stress space (Haigh–Westergaard coordinates), which are the volumetric effective stress

$$\bar{\sigma}_V = \frac{I_1}{3} \tag{41}$$

the norm of the deviatoric effective stress

$$\bar{\rho} = \sqrt{2J_2} \tag{42}$$

and the Lode angle

$$\bar{\theta} = \frac{1}{3} \arccos\left(\frac{3\sqrt{3}}{2} \frac{J_3}{J_2^{3/2}}\right) \tag{43}$$

The foregoing definitions use the first invariant

$$I_1 = \bar{\boldsymbol{\sigma}} : \boldsymbol{\delta} = \bar{\sigma}_{ij}\delta_{ij} \tag{44}$$

of the effective stress tensor $\bar{\boldsymbol{\sigma}}$, and the second and third invariants

$$J_2 = \tfrac{1}{2}\bar{\mathbf{s}} : \bar{\mathbf{s}} = \tfrac{1}{2}\bar{\mathbf{s}}^2 : \boldsymbol{\delta} = \tfrac{1}{2}\bar{s}_{ij}\bar{s}_{ij} \tag{45}$$

$$J_3 = \tfrac{1}{3}\bar{\mathbf{s}}^3 : \boldsymbol{\delta} = \tfrac{1}{3}\bar{s}_{ij}\bar{s}_{jk}\bar{s}_{ki} \tag{46}$$

of the deviatoric effective stress tensor $\bar{\mathbf{s}} = \bar{\boldsymbol{\sigma}} - \boldsymbol{\delta} I_1/3$.

The yield function

$$f_{\mathrm{p}}(\bar{\sigma}_{\mathrm{V}}, \bar{\rho}, \bar{\theta}; \kappa_{\mathrm{p}}) = \left\{ [1 - q_{\mathrm{h}}(\kappa_{\mathrm{p}})]\left(\frac{\bar{\rho}}{\sqrt{6}\bar{f}_{\mathrm{c}}} + \frac{\bar{\sigma}_{\mathrm{V}}}{\bar{f}_{\mathrm{c}}}\right)^2 + \sqrt{\frac{3}{2}}\frac{\bar{\rho}}{\bar{f}_{\mathrm{c}}}\right\}^2 + m_0 q_{\mathrm{h}}^2(\kappa_{\mathrm{p}})\left[\frac{\bar{\rho}}{\sqrt{6}\bar{f}_{\mathrm{c}}}r(\cos\bar{\theta}) + \frac{\bar{\sigma}_{\mathrm{V}}}{\bar{f}_{\mathrm{c}}}\right] - q_{\mathrm{h}}^2(\kappa_{\mathrm{p}})$$

(47)

depends on the effective stress (which enters in the form of cylindrical coordinates) and on the hardening variable κ_{p} (which enters through a dimensionless variable q_{h}). Parameter $\bar{f}_{\mathrm{c}}$ is the uniaxial compressive strength. Note that, under uniaxial compression characterized by axial stress $\bar{\sigma} < 0$, we have $\bar{\sigma}_{\mathrm{V}} = \bar{\sigma}/3$, $\bar{\rho} = -\sqrt{2/3}\bar{\sigma}$ and $\bar{\theta} = 60°$. The yield function then reduces to $f_{\mathrm{p}} = (\bar{\sigma}/\bar{f}_{\mathrm{c}})^2 - q_{\mathrm{h}}^2$. This means that function q_{h} describes the evolution of the uniaxial compressive yield stress normalized by its maximum value, $\bar{f}_{\mathrm{c}}$.

The meridians of the yield surface $f_{\mathrm{p}} = 0$ are parabolic, and the deviatoric sections change from triangular shapes at low confinement to almost circular shapes at high confinement. The shape of the deviatoric section is controlled by the function

$$r(\cos\bar{\theta}) = \frac{4(1 - e^2)\cos^2\bar{\theta} + (2e - 1)^2}{2(1 - e^2)\cos\bar{\theta} + (2e - 1)\sqrt{4(1 - e^2)\cos^2\bar{\theta} + 5e^2 - 4e}}$$

(48)

proposed by Willam and Warnke (1974) and later exploited by many authors, including Etse and Willam (1994), Menétrey and Willam (1995), Kang (1997) and Kang and Willam (1999). The eccentricity parameter e and the friction parameter m_0 are calibrated from the values of uniaxial and equibiaxial compressive strengths and uniaxial tensile strength; see Appendix A.2.

The shape of the meridians of the yield surface is controlled by the hardening variable q_{h} and the friction parameter m_0. The evolution of the yield surface during hardening is presented in Figs. 3 and 4. The maximum size of the elastic domain is attained when the variable q_{h} is equal to one (which is its maximum value, as follows from the hardening law, to be specified in (53)). The yield surface then turns into the failure surface proposed by Menétrey and Willam (1995) and described by the equation

$$f_{\mathrm{p}}(\bar{\sigma}_{\mathrm{V}}, \bar{\rho}, \bar{\theta}; 1) \equiv \frac{3}{2}\frac{\bar{\rho}^2}{\bar{f}_{\mathrm{c}}^2} + m_0\left(\frac{\bar{\rho}}{\sqrt{6}\bar{f}_{\mathrm{c}}}r(\cos\bar{\theta}) + \frac{\bar{\sigma}_{\mathrm{V}}}{\bar{f}_{\mathrm{c}}}\right) - 1 = 0$$

(49)

The yield function proposed in the present article and defined in (47) is an adapted version of the modified Leon model (Etse and Willam, 1994). The difference is that in the present formulation the function r enters only the linear part of the yield function. In this way a constant eccentricity parameter e can be used, but the shape of the deviatoric section still changes with increasing confinement.
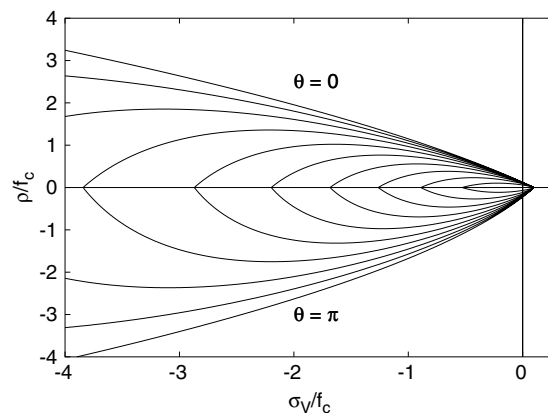

Fig. 3. The evolution of the meridional section of the yield surface during hardening.
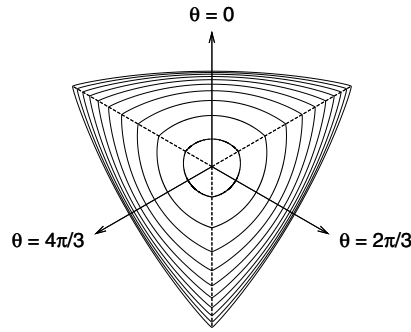
Fig. 4. The evolution of the deviatoric section of the yield surface during hardening for a constant volumetric stress of $\bar{\sigma}_{\mathrm{V}} = -\bar{f}_{\mathrm{c}}/3$.

3.1.2. Flow rule

In the present model, the flow rule

$$\dot{\boldsymbol{\varepsilon}}_{\mathrm{p}} = \dot{\lambda}\frac{\partial g_{\mathrm{p}}}{\partial \bar{\boldsymbol{\sigma}}} = \dot{\lambda}\mathbf{m} \tag{50}$$

is nonassociated, which means that the yield function f_{p} and the plastic potential g_{p} do not coincide and, therefore, the direction of the plastic flow $\mathbf{m} \equiv \partial g_{\mathrm{p}}/\partial \bar{\boldsymbol{\sigma}}$ is not normal to the yield surface. This is important for realistic modeling of the volumetric expansion under compression for frictional materials such as concrete. An associated flow rule for this type of yield surface gives an unrealistically high volumetric expansion in compression, which leads in the case of passive confinement to an overestimated strength (peak stress); see Grassl (2004).

The plastic potential is given as

$$g_{\mathrm{p}}(\bar{\sigma}_{\mathrm{V}}, \bar{\rho}; \kappa_{\mathrm{p}}) = \left\{ [1 - q_{\mathrm{h}}(\kappa_{\mathrm{p}})]\left(\frac{\bar{\rho}}{\sqrt{6}\bar{f}_{\mathrm{c}}} + \frac{\bar{\sigma}_{\mathrm{V}}}{\bar{f}_{\mathrm{c}}}\right)^2 + \sqrt{\frac{3}{2}}\frac{\bar{\rho}}{\bar{f}_{\mathrm{c}}} \right\}^2 + q_{\mathrm{h}}^2(\kappa_{\mathrm{p}})\left(\frac{m_0\bar{\rho}}{\sqrt{6}\bar{f}_{\mathrm{c}}} + \frac{m_{\mathrm{g}}(\bar{\sigma}_{\mathrm{V}})}{\bar{f}_{\mathrm{c}}}\right) \tag{51}$$

Parameter m_0 is constant and equal to the friction parameter in the yield function (47). The ratio of the volumetric and the deviatoric parts of the flow direction is controlled by function m_{g}, which depends on the volumetric stress and is defined as

$$m_{\mathrm{g}}(\bar{\sigma}_{\mathrm{V}}) = A_{\mathrm{g}}B_{\mathrm{g}}\bar{f}_{\mathrm{c}}\exp\frac{\bar{\sigma}_{\mathrm{V}} - \bar{f}_{\mathrm{t}}/3}{B_{\mathrm{g}}\bar{f}_{\mathrm{c}}} \tag{52}$$

where A_{g} and B_{g} are model parameters that are determined from assumptions on the plastic flow in uniaxial tension and compression; see Appendix A.

The plastic potential does not depend on the third Haigh–Westergaard coordinate (Lode angle $\bar{\theta}$). This increases the efficiency of the implementation (see Section 3.4) and the robustness of the model. However, it also limits the capability of this flow rule to describe the response of concrete in multiaxial compression.

3.1.3. Hardening law

The dimensionless variable q_{h} that appears in the yield function (47) is a function of the hardening variable κ_{p}. It controls the size and shape of the yield surface and, thereby, of the elastic domain.

The hardening law is given by

$$q_{\mathrm{h}}(\kappa_{\mathrm{p}}) = \begin{cases} q_{\mathrm{h}_0} + (1 - q_{\mathrm{h}_0})\kappa_{\mathrm{p}}(\kappa_{\mathrm{p}}^2 - 3\kappa_{\mathrm{p}} + 3) & \text{if } \kappa_{\mathrm{p}} < 1 \\ 1 & \text{if } \kappa_{\mathrm{p}} \geqslant 1 \end{cases} \tag{53}$$

The initial inclination of the hardening curve (at $\kappa_{\mathrm{p}} = 0$) is positive and finite, and the inclination at peak (i.e., at $\kappa_{\mathrm{p}} = 1$) is zero, as depicted in Fig. 5a.
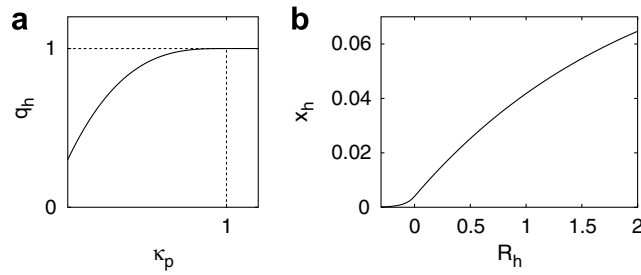
Fig. 5. (a) The hardening law. (b) The ductility measure for stress states on the compressive meridian. With increasing confinement the evolution of the hardening variable is slowed down.

3.1.4. Hardening variable

The evolution law for the hardening variable,

$$\dot{\kappa}_{\mathrm{p}} = \frac{\|\dot{\boldsymbol{\varepsilon}}_{\mathrm{p}}\|}{x_{\mathrm{h}}(\bar{\sigma}_{\mathrm{V}})} \cos^2 \bar{\theta} = \frac{\dot{\lambda}\|\mathbf{m}\|}{x_{\mathrm{h}}(\bar{\sigma}_{\mathrm{V}})} \cos^2 \bar{\theta} \tag{54}$$

sets the rate of the hardening variable equal to the norm of the plastic strain rate scaled by a hardening ductility measure

$$x_{\mathrm{h}}(\bar{\sigma}_{\mathrm{V}}) = \begin{cases} A_{\mathrm{h}} - (A_{\mathrm{h}} - B_{\mathrm{h}}) \exp(-R_{\mathrm{h}}(\bar{\sigma}_{\mathrm{V}})/C_{\mathrm{h}}) & \text{if } R_{\mathrm{h}}(\bar{\sigma}_{\mathrm{V}}) \geqslant 0 \\ E_{\mathrm{h}} \exp(R_{\mathrm{h}}(\bar{\sigma}_{\mathrm{V}})/F_{\mathrm{h}}) + D_{\mathrm{h}} & \text{if } R_{\mathrm{h}}(\bar{\sigma}_{\mathrm{V}}) < 0 \end{cases} \tag{55}$$

depicted in Fig. 5b. The dependence of the scaling factor x_{h} on the volumetric stress $\bar{\sigma}_{\mathrm{V}}$ is constructed such that the model response is more ductile under compression. The variable

$$R_{\mathrm{h}}(\bar{\sigma}_{\mathrm{V}}) = -\frac{\bar{\sigma}_{\mathrm{V}}}{\bar{f}_{\mathrm{c}}} - \frac{1}{3} \tag{56}$$

is a linear function of the volumetric effective stress. Model parameters A_{h}, B_{h}, C_{h} and D_{h} are calibrated from the values of strain at peak stress under uniaxial tension, uniaxial compression and triaxial compression, whereas the parameters E_{h} and F_{h} are determined from the conditions of a smooth transition between the two parts of Eq. (55) at $R_{\mathrm{h}} = 0$:

$$E_{\mathrm{h}} = B_{\mathrm{h}} - D_{\mathrm{h}} \tag{57}$$

$$F_{\mathrm{h}} = \frac{(B_{\mathrm{h}} - D_{\mathrm{h}})C_{\mathrm{h}}}{B_{\mathrm{h}} - A_{\mathrm{h}}} \tag{58}$$

To simplify notation, we introduce the function

$$k_{\mathrm{p}}(\bar{\boldsymbol{\sigma}}, \kappa_{\mathrm{p}}) = \frac{\|\mathbf{m}(\bar{\boldsymbol{\sigma}}, \kappa_{\mathrm{p}})\|}{x_{\mathrm{h}}(\bar{\boldsymbol{\sigma}} : \boldsymbol{\delta}/3)} \cos^2 \bar{\theta} \tag{59}$$

and rewrite (54) as

$$\dot{\kappa}_{\mathrm{p}} = \dot{\lambda} k_{\mathrm{p}}(\bar{\boldsymbol{\sigma}}, \kappa_{\mathrm{p}}) \tag{60}$$

3.2. Components of the damage model

The damage model is formulated in the framework of isotropic scalar damage. The main components are the loading function with the definition of the equivalent strain and the damage evolution law. In contrast to pure damage models with damage driven by the total strain, here the damage is linked to the evolution of plastic strain. The individual components are presented in the next paragraphs.
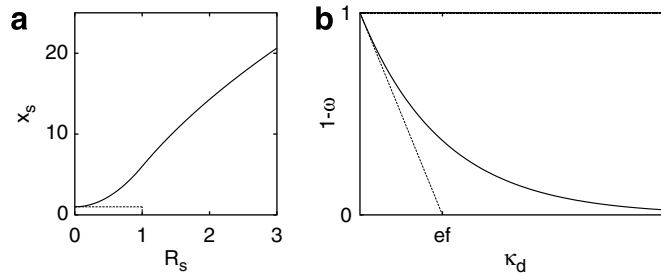
Fig. 6. (a) The softening ductility measure. With increasing principal negative strains the evolution of damage is slowed down. (b) Evolution of the scalar damage.

3.2.1. The loading function and the definition of the equivalent strain

The damage loading function has the form (6) but the equivalent strain $\tilde{\varepsilon}$ is not an explicit function of the strain or plastic strain. It is defined incrementally by the rate equation

$$\dot{\tilde{\varepsilon}} = \begin{cases} 0 & \text{if } \kappa_p < 1 \\ \dot{\varepsilon}_{pV}/x_s(\bar{\sigma}_V) & \text{if } \kappa_p \geqslant 1 \end{cases} \tag{61}$$

Here, $\dot{\varepsilon}_{pV} = \dot{\boldsymbol{\varepsilon}}_p : \boldsymbol{\delta}$ is the volumetric plastic strain rate and x_s is a softening ductility measure (Fig. 6a) defined as

$$x_s(\bar{\sigma}_V) = \begin{cases} 1 + A_s R_s^2(\bar{\sigma}_V) & \text{if } R_s(\bar{\sigma}_V) < 1 \\ 1 - 3A_s + 4A_s\sqrt{R_s(\bar{\sigma}_V)} & \text{if } R_s(\bar{\sigma}_V) \geqslant 1 \end{cases} \tag{62}$$

A_s is a model parameter determined from the softening response in uniaxial compression. The dimensionless variable $R_s = \dot{\varepsilon}_{pV}^-/\dot{\varepsilon}_{pV}$ is defined as the ratio between the "negative" volumetric plastic strain rate

$$\dot{\varepsilon}_{pV}^- = \sum_{I=1}^{3} \langle -\dot{\varepsilon}_{pI} \rangle \tag{63}$$

and the total volumetric plastic strain rate $\dot{\varepsilon}_{pV}$. Since this ratio depends only on the flow direction $\partial g_p/\partial\bar{\boldsymbol{\sigma}}$, R_s can be considered as a function of the effective stress. In (63), $\dot{\varepsilon}_{pI}$ are the principal components of the rate of plastic strains and $\langle \cdot \rangle$ denotes the McAuley brackets (positive-part operator). For uniaxial tension, for instance, all three principal plastic strain rates are nonnegative, and so $\dot{\varepsilon}_{pV}^- = 0$, $R_s = 0$ and $x_s = 1$. This means that under uniaxial tensile loading we have $\kappa_d = \kappa_p - 1$. On the other hand, under compressive stress states the negative principal plastic strain rates lead to a ductility measure x_s greater than one and the evolution of damage is slowed down. It should be emphasized that the flow rule for this specific model is constructed such that the volumetric part of plastic strain rate at the ultimate yield surface cannot be negative.

3.2.2. Evolution law

The evolution law g_d, which relates the damage variable ω to the internal variable κ_d, is assumed to have the exponential form

$$\omega = g_d(\kappa_d) = 1 - \exp(-\kappa_d/\varepsilon_f) \tag{64}$$

where ε_f is a parameter that controls the slope of the softening curve; see Fig. 6b.

3.3. Thermodynamic aspects

The constitutive equations have been constructed without any reference to a thermodynamic framework. The reason is that a realistic description of dilatancy in concrete requires a nonassociated flow rule, and therefore the present model does not belong to the class of generalized standard materials. Therefore, the results of Contrafatto and Cuomo (2002) are not applicable. For nonstandard materials, the evolution laws for internal

variables are not derived from a dissipation potential but are simply postulated. Still, it is useful to check whether the resulting model satisfies the dissipation inequality. The condition of nonnegative dissipation may lead to certain constraints on the model parameters, which should be respected to make sure that the model remains thermodynamically admissible.

First of all, we need to specify the expression for the free energy. For the present type of damage-plastic model, the most natural choice for specific free energy (per unit volume) is

$$\rho\psi(\boldsymbol{\varepsilon}, \boldsymbol{\varepsilon}_\mathrm{p}, \omega) = \tfrac{1}{2}(1 - \omega)(\boldsymbol{\varepsilon} - \boldsymbol{\varepsilon}_\mathrm{p}) : \mathbf{D}_\mathrm{e} : (\boldsymbol{\varepsilon} - \boldsymbol{\varepsilon}_\mathrm{p}) \tag{65}$$

Here, ρ is the density (specific mass), ψ is the Helmholtz free energy per unit mass, and we consider isothermal processes, so that the temperature remains constant and is not explicitly listed among the state variables. The rate of dissipation per unit volume is then evaluated as

$$\mathscr{D} = \boldsymbol{\sigma} : \dot{\boldsymbol{\varepsilon}} - \rho\dot{\psi} = \left(\boldsymbol{\sigma} - \rho\frac{\partial\psi}{\partial\boldsymbol{\varepsilon}}\right) : \dot{\boldsymbol{\varepsilon}} - \rho\frac{\partial\psi}{\partial\boldsymbol{\varepsilon}_\mathrm{p}} : \dot{\boldsymbol{\varepsilon}}_\mathrm{p} - \rho\frac{\partial\psi}{\partial\omega}\dot{\omega} \tag{66}$$

Using standard arguments we obtain the stress–strain equation

$$\boldsymbol{\sigma} = \rho\frac{\partial\psi}{\partial\boldsymbol{\varepsilon}} = (1 - \omega)\mathbf{D}_\mathrm{e} : (\boldsymbol{\varepsilon} - \boldsymbol{\varepsilon}_\mathrm{p}) \tag{67}$$

and the dissipation inequality

$$\mathscr{D} = -\rho\frac{\partial\psi}{\partial\boldsymbol{\varepsilon}_\mathrm{p}} : \dot{\boldsymbol{\varepsilon}}_\mathrm{p} - \rho\frac{\partial\psi}{\partial\omega}\dot{\omega} = (1 - \omega)(\boldsymbol{\varepsilon} - \boldsymbol{\varepsilon}_\mathrm{p}) : \mathbf{D}_\mathrm{e} : \dot{\boldsymbol{\varepsilon}}_\mathrm{p} + \frac{1}{2}(\boldsymbol{\varepsilon} - \boldsymbol{\varepsilon}_\mathrm{p}) : \mathbf{D}_\mathrm{e} : (\boldsymbol{\varepsilon} - \boldsymbol{\varepsilon}_\mathrm{p})\dot{\omega} = \boldsymbol{\sigma} : \dot{\boldsymbol{\varepsilon}}_\mathrm{p} + Y\dot{\omega} \geqslant 0 \tag{68}$$

where the dissipative thermodynamic force conjugate to the plastic strain is $-\rho\frac{\partial\psi}{\partial\boldsymbol{\varepsilon}_\mathrm{p}} : \dot{\boldsymbol{\varepsilon}}_\mathrm{p} = (1 - \omega)\mathbf{D}_\mathrm{e} : (\boldsymbol{\varepsilon} - \boldsymbol{\varepsilon}_\mathrm{p})$, which turns out to be equal to the (nominal) stress $\boldsymbol{\sigma}$, and the dissipative force conjugate to the damage variable is the damage energy release rate

$$Y = -\rho\frac{\partial\psi}{\partial\omega} = \frac{1}{2}(\boldsymbol{\varepsilon} - \boldsymbol{\varepsilon}_\mathrm{p}) : \mathbf{D}_\mathrm{e} : (\boldsymbol{\varepsilon} - \boldsymbol{\varepsilon}_\mathrm{p}) \tag{69}$$

which is equal to the specific free energy of the undamaged material under the same elastic strain. The terms $\boldsymbol{\sigma} : \dot{\boldsymbol{\varepsilon}}$ and $Y\dot{\omega}$ can be interpreted as the plastic dissipation and damage dissipation, respectively. In principle, only the total dissipation must be nonnegative, and since the damage growth is in the present model not completely independent of the plastic flow, the individual parts of dissipation do not necessarily need to be nonnegative. However, we will require that each of them be nonnegative, which is a sufficient but not necessary condition for thermodynamic admissibility.

The damage part of dissipation $Y\dot{\omega}$ is always nonnegative, because $Y \geqslant 0$ and the damage variable ω cannot decrease, i.e. $\dot{\omega} \geqslant 0$ (in fact, this is the constraint on the evolution law, but it is automatically satisfied). Therefore, we focus on the plastic dissipation

$$\mathscr{D}_\mathrm{p} = \boldsymbol{\sigma} : \dot{\boldsymbol{\varepsilon}}_\mathrm{p} = \dot{\lambda}\boldsymbol{\sigma} : \frac{\partial g_\mathrm{p}}{\partial\bar{\boldsymbol{\sigma}}} = \dot{\lambda}(1 - \omega)\bar{\boldsymbol{\sigma}} : \frac{\partial g_\mathrm{p}}{\partial\bar{\boldsymbol{\sigma}}} \tag{70}$$

Since $\dot{\lambda}$ and $1 - \omega$ are both nonnegative, it remains to verify that the scalar product of the effective stress and the plastic flow direction is nonnegative.

It is easy to see that the plastic potential defined in (51) is a convex function of the stress invariants $\bar{\sigma}_\mathrm{V}$ and $\bar{\rho}$ (with the hardening variable κ_p taken as a constant parameter). Moreover, with some mild assumptions regarding the model parameters, it is possible to prove that for all states that satisfy the yield condition $f_\mathrm{p}(\bar{\sigma}_\mathrm{V}, \bar{\rho}, \bar{\theta}; \kappa_\mathrm{p}) = 0$ the value of the plastic potential $g_\mathrm{p}(\bar{\sigma}_\mathrm{V}, \bar{\rho}; \kappa_\mathrm{p})$ is larger than $g_\mathrm{p}(0, 0; \kappa_\mathrm{p})$; for a rigorous proof see Appendix C. According to the theory of convex functions, these two properties guarantee that the scalar product of vector $(\bar{\sigma}_\mathrm{V}, \bar{\rho})$ with the gradient of g_p evaluated at $(\bar{\sigma}_\mathrm{V}, \bar{\rho})$ is nonnegative, which is exactly what we need in order to prove that $\mathscr{D}_\mathrm{p} \geqslant 0$. The mild conditions on the parameters do not represent any practical restriction. The proposed model is therefore fully thermodynamically consistent and there is no danger that e.g. cyclic loading would lead to spurious generation of energy instead of energy dissipation.

3.4. Implementation

The present constitutive model has been implemented within the framework of the nonlinear finite element method, with the continuous loading process is replaced by incremental time steps. In each step the boundary value problem (global level) and the integration of the constitutive laws (local level) are solved.

For the boundary value problem on the global level, the usual incremental-iterative solution strategy is used, either in the form of the standard Newton–Raphson iteration with the algorithmic tangent stiffness, or in a modified form with the tangent stiffness replaced by the secant stiffness

$$\mathbf{D}_s = (1 - \omega)\mathbf{D}_e \tag{71}$$

In the former case, the convergence rate is quadratic but divergence may occur in steps during which localization of the inelastic deformation occurs. In the latter case, the convergence rate is only linear, but the method is more robust. Derivation of the algorithmic ("consistent") tangent stiffness is given in Appendix B.

For the local problem, the updated values $(\cdot)^{(n+1)}$ of the stress and the internal variables at the end of the step are obtained by a fully implicit (backward Euler) integration of the rate form of the constitutive equations, starting from their known values $(\cdot)^{(n)}$ at the beginning of the step and applying the given strain increment $\Delta\varepsilon = \varepsilon^{(n+1)} - \varepsilon^{(n)}$. The integration scheme is divided into two sequential steps, corresponding to the plastic and damage parts of the model. In the plastic part, the plastic strain ε_p and the effective stress $\bar{\sigma}$ at the end of the step are determined. In the damage part, the damage variable ω and the nominal stress σ at the end of the step are obtained. To simplify the notation, superscripts $(n+1)$ denoting the state at the end of the step are dropped from the subsequent derivations.

3.4.1. Plasticity part

The plastic part of the stress evaluation algorithm is based on the standard split into an elastic predictor and a plastic corrector using the backward Euler scheme. The state at the beginning of the step is assumed to be given, same as the strain increment. The unknowns to be determined are the stress $\bar{\sigma}$, plastic strain ε_p and plastic hardening variable κ_p at the end of the step, and the increment of the plastic multiplier, $\Delta\lambda$. They must satisfy the stress–strain equation

$$\bar{\sigma} = \mathbf{D}_e : (\varepsilon - \varepsilon_p) \tag{72}$$

the incremental loading–unloading conditions

$$f_p(\bar{\sigma}, \kappa_p) \leqslant 0, \quad \Delta\lambda \geqslant 0, \quad \Delta\lambda f_p(\bar{\sigma}, \kappa_p) = 0 \tag{73}$$

and the discretized form of the evolution laws

$$\varepsilon_p = \varepsilon_p^{(n)} + \Delta\lambda \mathbf{m}(\bar{\sigma}, \kappa_p) \tag{74}$$

$$\kappa_p = \kappa_p^{(n)} + \Delta\lambda k_p(\bar{\sigma}, \kappa_p) \tag{75}$$

The plastic strain ε_p is eliminated from the problem by substituting (74) into (72). The resulting equation can be written as

$$\bar{\sigma} = \mathbf{D}_e : [\varepsilon - \varepsilon_p^{(n)} - \Delta\lambda \mathbf{m}(\bar{\sigma}, \kappa_p)] = \bar{\sigma}^{tr} - \Delta\lambda \mathbf{D}_e : \mathbf{m}(\bar{\sigma}, \kappa_p) \tag{76}$$

where $\bar{\sigma}^{tr} = \mathbf{D}_e : (\varepsilon - \varepsilon_p^{(n)}) = \bar{\sigma}^{(n)} + \mathbf{D}_e : \Delta\varepsilon$ is the trial stress, easily evaluated from the given strain increment. If the trial stress is not outside the yield surface, i.e., if $f_p(\bar{\sigma}^{tr}, \kappa_p^{(n)}) \leqslant 0$, the step is elastic and we set $\Delta\lambda = 0$, $\bar{\sigma} = \bar{\sigma}^{tr}$, $\varepsilon_p = \varepsilon_p^{(n)}$ and $\kappa_p = \kappa_p^{(n)}$. If the trial stress is outside the yield surface, the unknowns $\bar{\sigma}$, κ_p and $\Delta\lambda$ are determined from the set of nonlinear equations consisting of (75) and (76) and the yield condition

$$f_p(\bar{\sigma}, \kappa_p) = 0 \tag{77}$$

For the particular type of plastic potential considered here, the number of unknowns and equations can be further reduced. First, since the plastic potential g_p is an isotropic function of stress, its gradient $\mathbf{m}$ has the same principal directions as the stress tensor $\bar{\sigma}$ for which it is evaluated. The elastic stiffness is also considered to be isotropic, and so it follows from (76) that the principal directions of the stress $\bar{\sigma}$ at the step end coincide

with the principal directions of the trial stress $\bar{\boldsymbol{\sigma}}^{\mathrm{tr}}$. These directions can be determined in advance, and the stress is then fully characterized by three principal values instead of six general components. The tensorial equation (76) is replaced by three scalar equations written for the principal stresses. Second, since the plastic potential g_{p} defined in (51) depends only on stress invariants $\bar{\sigma}_{\mathrm{V}}$ and $\bar{\rho}$ but not on the Lode angle $\bar{\theta}$, it can be shown that the trial stress $\bar{\boldsymbol{\sigma}}^{\mathrm{tr}}$, actual stress at the step end $\bar{\boldsymbol{\sigma}}$ and the gradient $\mathbf{m}$ of the plastic potential all have the same Lode angle $\bar{\theta} = \theta^{\mathrm{tr}}$, which can be evaluated directly from the trial state. So Eq. (76) is finally replaced by two scalar equations for the stress invariants

$$\bar{\sigma}_{\mathrm{V}} = \bar{\sigma}_{\mathrm{V}}^{\mathrm{tr}} - K \Delta\lambda m_{\mathrm{V}}(\bar{\boldsymbol{\sigma}}, \kappa_{\mathrm{p}}) \tag{78}$$
$$\bar{\rho} = \bar{\rho}^{\mathrm{tr}} - 2G \Delta\lambda m_{\mathrm{D}}(\bar{\boldsymbol{\sigma}}, \kappa_{\mathrm{p}}) \tag{79}$$

where $m_{\mathrm{V}} = \mathbf{m} : \boldsymbol{\delta}$ and $m_{\mathrm{D}} = \|\mathbf{m} - m_{\mathrm{V}}\boldsymbol{\delta}/3\|$ are invariants of the flow direction $\mathbf{m}$, $K = E/3(1 - 2\nu)$ is the elastic bulk modulus, and $G = E/2(1 + \nu)$ is the elastic shear modulus.

The set of four nonlinear equations (75) and (77)–(79) with unknowns $\bar{\sigma}_{\mathrm{V}}$, $\bar{\rho}$, $\Delta\lambda$ and κ_{p} is solved by the Newton–Raphson method, starting from the initial guess $\bar{\sigma}_{\mathrm{V}} = \bar{\sigma}_{\mathrm{V}}^{\mathrm{tr}}$, $\bar{\rho} = \bar{\rho}^{\mathrm{tr}}$, $\Delta\lambda = 0$ and $\kappa_{\mathrm{p}} = \kappa_{\mathrm{p}}^{(n)}$. Once the stress invariants $\bar{\sigma}_{\mathrm{V}}$ and $\bar{\rho}$ are computed, the principal stresses $\bar{\sigma}_I$, $I = 1, 2, 3$, can be evaluated as follows:

$$\begin{Bmatrix} \bar{\sigma}_1 \\ \bar{\sigma}_2 \\ \bar{\sigma}_3 \end{Bmatrix} = \bar{\sigma}_{\mathrm{V}} \begin{Bmatrix} 1 \\ 1 \\ 1 \end{Bmatrix} + \sqrt{\frac{2}{3}}\bar{\rho} \begin{Bmatrix} \cos\theta^{\mathrm{tr}} \\ \cos(\theta^{\mathrm{tr}} - 2\pi/3) \\ \cos(\theta^{\mathrm{tr}} + 2\pi/3) \end{Bmatrix} \tag{80}$$

Finally, substituting the principal stresses into the spectral decomposition

$$\bar{\boldsymbol{\sigma}} = \sum_{I=1}^{3} \bar{\sigma}_I \mathbf{n}_I \otimes \mathbf{n}_I \tag{81}$$

where $\mathbf{n}_I$, $I = 1, 2, 3$, are unit eigenvectors of the trial stress tensor and $\otimes$ denotes direct product, we construct the stress tensor at the end of the step. Of course, this is the effective stress, which should later be multiplied by the term $1 - \omega$ to obtain the nominal stress.

The yield surface corresponding to the yield function (47) has vertices at the intersections of the meridians with the hydrostatic axis. The vertices need special treatment, since the flow direction at these points is not unique. First, it is checked whether the stress state lies in a region that might require a vertex return. If the stress state is in such a region, then the vertex return is performed under the assumption that the final stress state lies on the hydrostatic axis ($\bar{\rho} = 0$). In that case, the yield condition is written in terms of the volumetric effective stress alone, and the volumetric effective stress that satisfies the yield condition is determined by the bisection method. Once the volumetric effective stress is known, it is checked whether the plastic strain increment is inside the cone bounded by the directions that correspond to the regular return according to Eq. (50) (for points in the immediate neighborhood of the vertex). If the plastic strain increment calculated under the assumption of vertex return is outside the cone, the assumption is abandoned and regular return is performed.

3.4.2. Damage part

Numerical treatment of the damage part of the constitutive model is very efficient since the rate form of the equivalent strain evolution in (61) is defined in terms of the plastic strain rate. The plastic strain is determined by the plasticity algorithm described in the previous section. The equivalent strain

$$\tilde{\varepsilon} = \tilde{\varepsilon}^{(n)} + \frac{\Delta\lambda m_{\mathrm{V}}(\bar{\boldsymbol{\sigma}}, \kappa_{\mathrm{p}})}{x_{\mathrm{s}}(\bar{\sigma}_{\mathrm{V}})} \tag{82}$$

is then evaluated from the incremental form of the evolution equation (61). Since $\tilde{\varepsilon}$ cannot decrease, we have $\kappa_{\mathrm{d}} = \tilde{\varepsilon}$ and $\omega = g_{\mathrm{d}}(\tilde{\varepsilon})$. Finally, the nominal stress is computed as

$$\boldsymbol{\sigma} = (1 - \omega)\bar{\boldsymbol{\sigma}} \tag{83}$$

using the damage variable ω and the effective stress $\bar{\boldsymbol{\sigma}}$.

4. Comparison with experimental results

4.1. Proportional loading

In the present section, the response of the constitutive model is compared to results of experiments in uniaxial, biaxial and triaxial compression and uniaxial tension for different types of concrete. The model parameters are summarized in Appendix A. In the following comparison only the parameters E, v, $\bar{f}_c$, $\bar{f}_t$ and ε_f are varied for the different sets of experimental results, according to the material properties extracted from the experiments. In all the cases, parameter A_s is set to 15. All other parameters are set to their default values mentioned in Appendix A.

Firstly, the model response is compared to uniaxial and biaxial compression tests (Kupfer et al., 1969), cf. Fig. 7. The model parameters are set to $E = 32$ GPa, $v = 0.18$, $\bar{f}_c = 32.8$ MPa, $\bar{f}_t = 3.3$ MPa and $\varepsilon_f = 165 \times 10^{-6}$.

Next, the model response is compared to triaxial compression tests with lateral confinement varying from 0 to 43 MPa, reported by Imran and Pantazopoulou (1996), cf. Fig. 8. The model parameters are set to $E = 30$ GPa, $v = 0.15$, $\bar{f}_c = 47.4$ MPa, $\bar{f}_t = 4.74$ MPa and $\varepsilon_f = 210 \times 10^{-6}$.
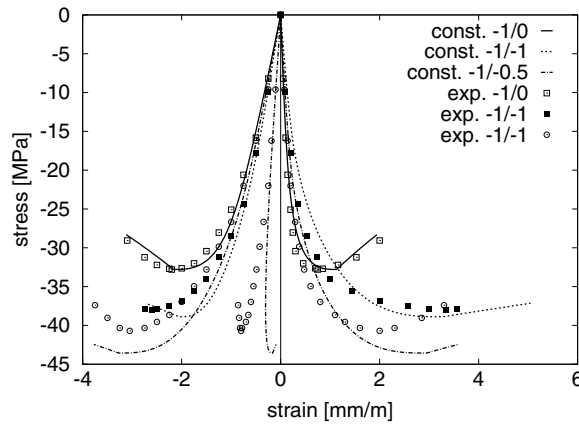

Fig. 7. The model response in uniaxial and biaxial compression with stress ratios of $-1/-0.5$ and $-1/-1$ compared to experimental results reported by Kupfer et al. (1969).
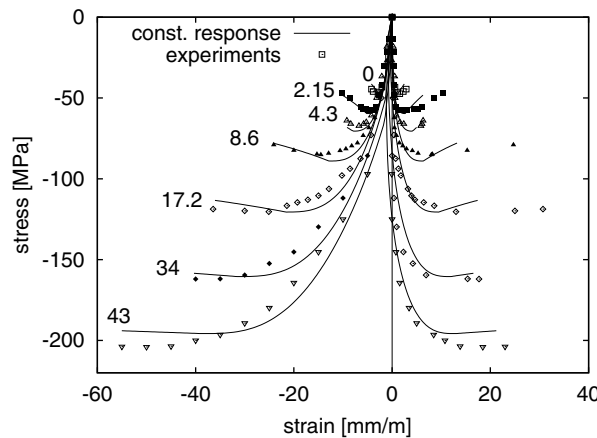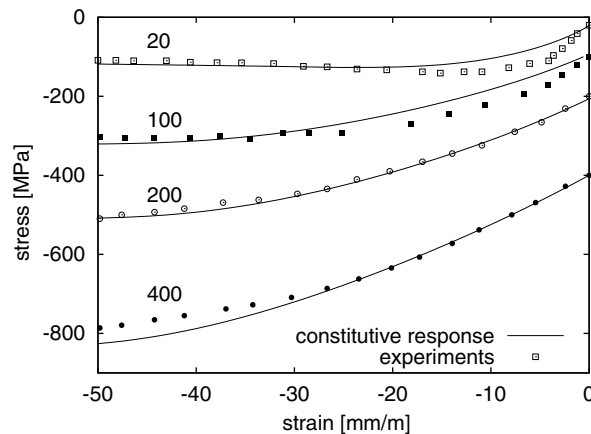

Fig. 8. The model response in triaxial compression with lateral confinement varying between 0 and 43 MPa compared to experimental results reported by Imran and Pantazopoulou (1996).

Additionally, experiments with high lateral confinement and with hydrostatic compression reported by Caner and Bažant (2000) are modeled; cf. Figs. 9 and 10. For this type of concrete, the model parameters are set to $E = 25$ GPa, $v = 0.2$, $\bar{f}_c = 45.7$ MPa, $\bar{f}_t = 4.57$ MPa and $\varepsilon_f = 210 \times 10^{-6}$. The constitutive response is also compared to experimental results of concrete subjected to uniaxial tension with unloading and reloading (Fig. 11) reported by Gopalaratnam and Shah (1985). The model parameters are set to $E = 28$ GPa, $v = 0.2$, $\bar{f}_c = 40$ MPa, $\bar{f}_t = 3.5$ MPa and $\varepsilon_f = 130 \times 10^{-6}$. Finally, the response of concrete subjected to uniaxial compression with unloading and reloading, reported by Karsan and Jirsa (1969), is modeled; see Fig. 12b. Here, the model parameters are set to $E = 30$ GPa, $v = 0.2$, $\bar{f}_c = 28$ MPa, $\bar{f}_t = 2.8$ MPa and $\varepsilon_f = 110 \times 10^{-6}$.

The overall agreement of the constitutive response with the wide range of experimental results, from cyclic tension to hydrostatic compression, is good. The lateral expansion in uniaxial compression is very well captured by the proposed nonassociated flow rule. Certain discrepancies are found in the comparison with the biaxial compression tests in Fig. 7, where the lateral positive strains in biaxial compression are overestimated. These results could be improved by including the Lode angle in the formulation of the plastic potential. However, the simplified version of the plastic potential is preferred because it increases robustness and efficiency of the numerical scheme.

The analyses of triaxial compression tests with low to medium confinement show a good agreement with the experimental results in strength and axial strain; see Fig. 8. The lateral strain under low confinement is

Fig. 9. The model response in triaxial compression with lateral confinement varying from 20 to 400 MPa compared to experimental results taken from Caner and Bažant (2000).
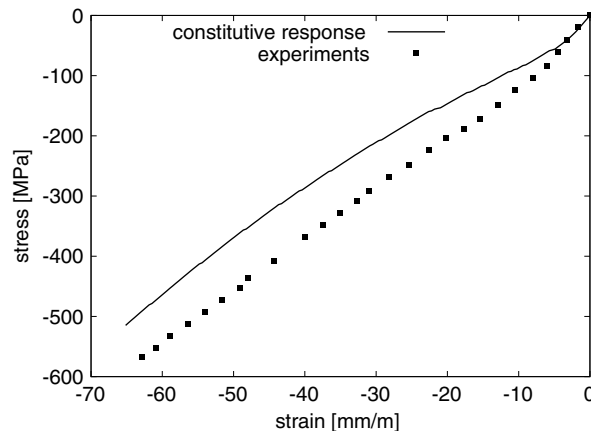
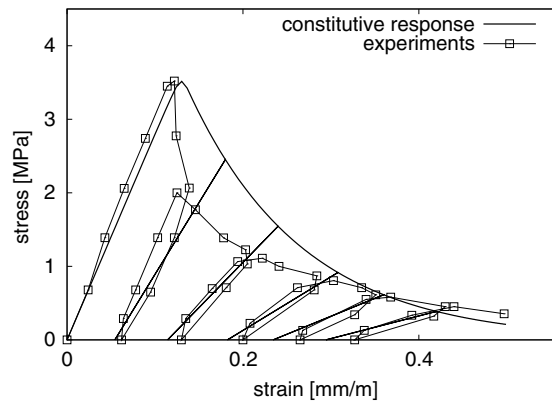Fig. 10. The model response in hydrostatic compression compared experimental results taken from Caner and Bažant (2000).

Fig. 11. The model response in cyclic uniaxial tension compared to experimental results reported by Gopalaratnam and Shah (1985).

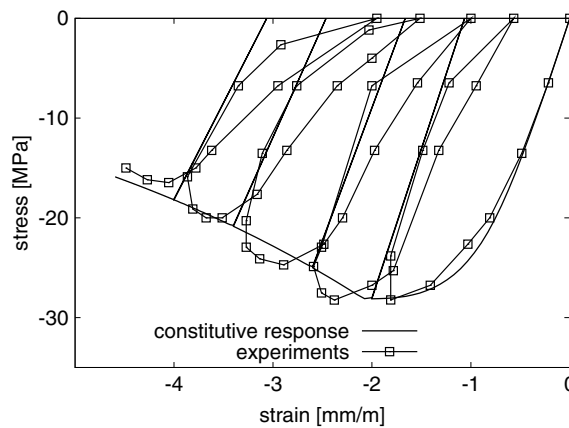

Fig. 12. The model response in cyclic uniaxial compression compared to experimental results reported by Karsan and Jirsa (1969).

somewhat underestimated by the model, which is also a consequence of the circular deviatoric section of the plastic potential. Very good agreement is obtained for the highly confined tests in Fig. 9, since the plasticity model predicts plastic flow close to the hydrostatic axis.

For hydrostatic compression, the behavior is also in qualitative agreement with the experimental results; see Fig. 10. Moreover, the model is able to describe the behavior in cyclic tension; see Fig. 11. The strength reduction in the initial part of the softening curve is underestimated, but the unloading stiffness at different levels of softening is captured very well. For cyclic compression, the agreement of the softening envelope and the initial unloading stiffness is good.

4.2. Nonproportional loading

In addition to monotonic and cyclic tests with proportional loading, the response of the proposed model was studied for a specific type of nonproportional loading, which can reveal important differences in the behavior of various constitutive models. In particular, loading by uniaxial compression followed by shear was considered. This type of loading path is related to the experiments reported by Caner et al. (2002), who tested plain concrete cylinders that were first compressed along their axis and then twisted at constant axial strain. The change of loading from compression to torsion occurred either at the peak of the uniaxial compressive stress–strain curve (at axial strain 2×10^{-3}), or at a state far in the postpeak range (at mean axial strain 4.5×10^{-3}). The tests revealed a strong reduction of the initial torsional stiffness as compared to the elastic stiffness. This phenomenon cannot be captured by a simple plasticity theory with a smooth yield surface

corresponding to an isotropic yield function. The reason is that at the point in the stress space corresponding to uniaxial compression, the shear stress increment is tangential to the yield surface (no matter which isotropic yield criterion is used). The initial response after the change of loading direction thus corresponds to neutral loading and activates the elastic stiffness. To obtain an immediate plastic yielding with reduced tangent stiffness, one would need to admit that the yield surface is not smooth but has a vertex; this is why the experimentally observed phenomenon is sometimes called the vertex effect. It is well known in the literature on metals (Bleich, 1952; Gerard and Becker, 1957) but for concrete it has been explored only recently.

Caner et al. (2002) performed also numerical analysis of their tests, using a fracture-plastic material model (Červenka et al., 1998) and version M4 of the micro-plane model (Bažant et al., 2000; Caner and Bažant, 2000). They simulated the entire specimen by finite elements using both models, and they also ran a simplified one-dimensional analysis using the micro-plane model. The conclusion was that the fracture-plastic model does not capture the vertex effect at all while the micro-plane model can reproduce it very well. On the other hand, the predictions of the ultimate value of torque were better with the former model while the latter over-predicted it by 40–50%.

In the present paper, the emphasis is not on exact fitting of the experimental results, but an illustration of the main features of the damage-plastic model. Therefore, instead of full three-dimensional analysis of the specimen, we construct the stress–strain curves for nonproportional loading that consists of compression in the x-direction followed by shear in the xy-plane. During both stages, it is assumed that the normal stress components σ_y and σ_z vanish. This is realistic for the first stage, but for the second stage it is just a simplification. Nevertheless, from the obtained shear stress–strain curve we can construct the torque–rotation relation using the formula
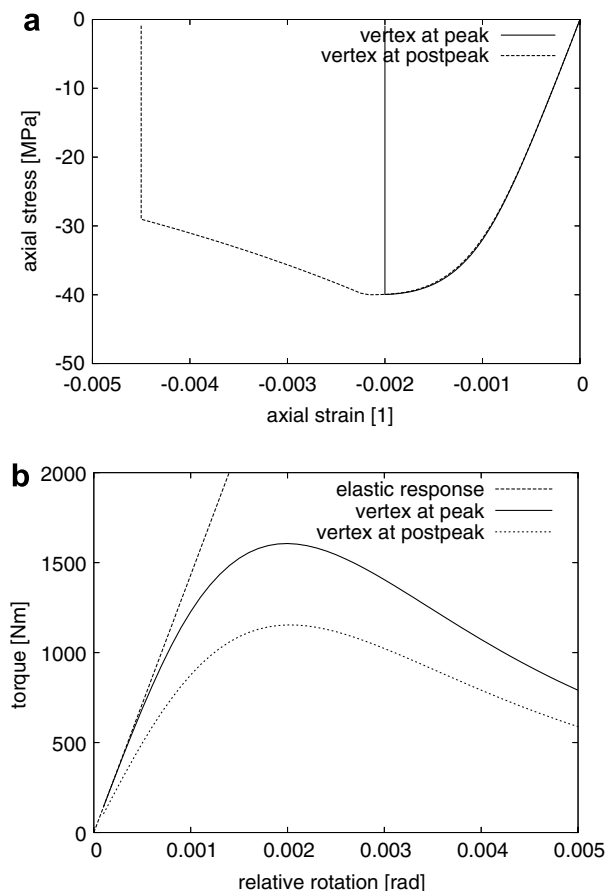

Fig. 13. Nonproportional loading: (a) first stage – compressive stress–strain curve, (b) second stage – torsional moment–rotation curve.

$$T(\varphi) = 2\pi \int_0^R r^2 \tau\left(\frac{\varphi r}{L}\right) \mathrm{d}r \tag{84}$$

in which T is the torque, φ is the relative rotation measured on gauge length $L = 114.3$ mm, $R = 50.8$ mm is the radius of the cylindrical specimen, $\tau(\gamma)$ is the shear stress evaluated at shear strain $\gamma = \varphi r/L$, and r is the integration variable corresponding to distance from the cylinder axis and changing from 0 to R. The analysis has been run with the default values of the model parameters, only the elastic properties $E = 36.9$ GPa and $v = 0.18$ and compressive strength $\bar{f}_c = 40$ MPa have been set to values reported by Caner et al. (2002) and parameter $\varepsilon_f = 0.25 \times 10^{-3}$ controlling the fracture energy has been adjusted so as to obtain a realistic post-peak slope of the uniaxial compressive curve.

The results are summarized in Fig. 13. For change of loading direction at the peak of the compressive curve, the initial torsional stiffness 1431 kN m/rad is equal to the elastic one, but for the change at postpeak it is reduced to 1038 kN m/rad. This reduction is due to damage and is less dramatic than the experimentally observed one, but it could be increased by modifying the assumption of perfectly plastic postpeak response of the plastic part of the model. The predicted ultimate torque is $T_{\mathrm{max},1} = 1605$ N m for change of loading direction at peak and $T_{\mathrm{max},2} = 1154$ N m for change at postpeak. The mean values measured in experiments were 2124 N m and 1078 N m, respectively. So the ultimate torque for change at peak is underpredicted but the relative errors are not larger than for the micro-plane model, which gave 2700 N m and 1460 N m, respectively. However, it must be admitted that the present model predicts a much more brittle response than the experiments (while the micro-plane model is more ductile). To obtain better agreement, modifications of the model parameters or even of certain model equations would be needed. This will be the subject of further investigations.

5. Structural example

The present damage-plastic model has been used in an analysis of reinforced concrete columns tested by Nemecek et al. (2005). The columns are subjected to a compressive force with a small eccentricity equal to 1/10 of the cross-sectional depth. In the experimental study the amount of lateral reinforcement and the concrete strength were varied. Here, only specimens of normal-strength concrete are analyzed. The geometry of the specimens and the loading setup are presented in Fig. 14a. The longitudinal spacing of the stirrups in the middle part of the specimen ranges between 50 and 150 mm. The corresponding tests are denoted as N50, N100 and N150.

The three-dimensional finite element model consists of linear hexahedral finite elements for concrete and three-dimensional beam elements with material and geometrical nonlinearities for the reinforcement. The finite element mesh is depicted in Fig. 14b. The number of elements ranges from 10,024 to 10,280 depending on the spacing of the stirrups. The outer ends of the columns are modeled by isotropic elasticity. For the middle part, where failure takes place, the proposed damage-plastic model is used. The material parameters are
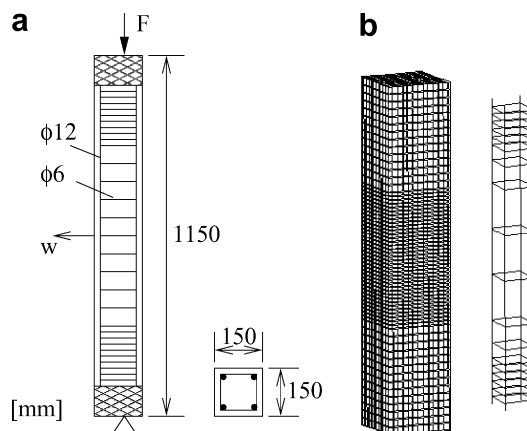

Fig. 14. Geometry, loading setup and finite element mesh of the reinforced concrete columns subjected to eccentric compression.
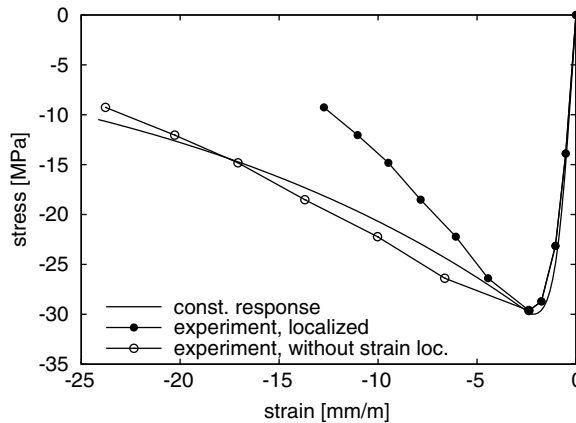
Fig. 15. The constitutive response in uniaxial compression compared to the experimental results.

determined from the average stress–strain curve in uniaxial compression and the mean compressive strength $\bar{f}_c = 30$ MPa. According to CEB (1991), other material parameters are estimated as tensile strength $f_t = 2.4$ MPa, Young's modulus $E = 31$ GPa and fracture energy $G_f = 54$ N/m.

The fracture energy is used to determine the control parameter of the softening curve in uniaxial tension $\varepsilon_f = 0.00525$, assuming that the longitudinal reinforcement leads to a localized strain profile distributed over several elements. A similar approach is adopted for the softening curve in compression. The average stress–strain curve available from the experimental study has been obtained on a 300 mm high concrete cylinder subjected to centric compression. Following the approach of Markeset and Hilleborg (1995), albeit not rigidly, a part of the vertical inelastic displacement in the postpeak regime is assumed to be localized and the remaining part is distributed equally over the height of the specimen. Therefore, the inelastic postpeak deformation is extracted from the average stress–strain curve and transformed into a strain over half of the specimen height; cf. Fig. 15. This stress–strain curve is used to determine the parameter A_s in the ductility measure of the damage model, which controls the relation between the softening curves in uniaxial tension and uniaxial compression. The use of a local stress–strain relation with softening leads in many cases to a mesh size-dependent solution, since the zone of localized strains depends on the element size. However, in an earlier study by Grassl and Lundgren (2003) it was observed that for this type of analysis the zone of localized strains is diffuse and does not depend on the element size. The parameter controlling the axial plastic strain at peak in uniaxial compression was set to $B_h = 0.0033$. The other parameters were set to their default values as listed in Appendix A.

The load–displacement curves for the analyses of the three specimens with different amount of lateral reinforcement are compared to the experimental results in Fig. 16. The load capacity and the deformations at peak
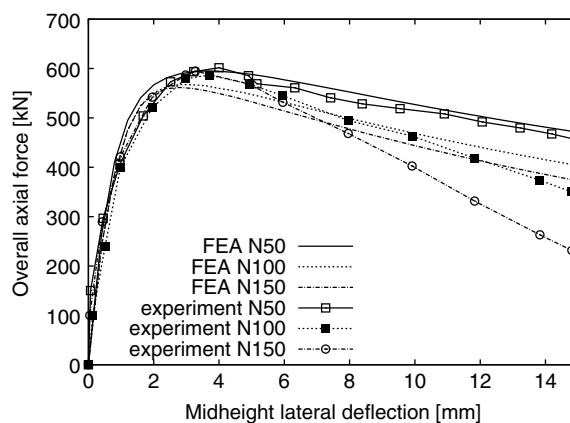

Fig. 16. The results of the analysis of the reinforced concrete columns in eccentric compression compared to the experiments.

are captured well. In the postpeak range, the model predicts qualitatively the correct trend – decreasing ductility for larger spacing of stirrups – but this effect is quantitatively underestimated.

6. Conclusions

The present study on the combination of stress-based plasticity and isotropic damage for modeling concrete failure has led to the following conclusions:

- For damage-plastic models with the plastic part based on the effective stress, local uniqueness is always guaranteed (provided that it is guaranteed for the plastic part only). This is not always the case for models with the plastic part based on the nominal stress.
- The combination of plasticity based on the effective stress and isotropic damage driven by the plastic strain has been shown to be suitable for predicting the failure of concrete in a wide range of loading cases from uniaxial tension to triaxial compression.
- The damage-plastic model can partially capture the reduction of shear stiffness due to previous compressive loading.
- The model is thermodynamically consistent and the algorithmic stiffness matrix is available.
- The model is suitable for three-dimensional structural applications and seems to predict reasonably well the response of reinforced concrete columns under eccentric compression.

Appendix A. Model parameters

A.1. Material properties

The damage-plastic model proposed in this paper has a large number of parameters, but not all of them are independent. Certain parameters are introduced just to simplify the notation and are directly linked to the other parameters by explicit expressions. Certain other parameters can be conveniently determined from suitable assumptions, or taken by their recommended default values. So the calibration procedure requires as input only a limited number of material properties, summarized in Table 1.

If no experimental results are available, it is sufficient to know the uniaxial compressive strength and determine the other properties from empirical formulas or take them by default values. For instance, according to the CEB-FIP Model Code (CEB, 1991), the uniaxial tensile strength can be estimated from the uniaxial compressive strength using the empirical relation

Table 1
Material properties needed for calibration

E	Young's modulus
v	Poisson's ratio
$\bar{f}_t$	Uniaxial tensile strength
$\bar{f}_c$	Uniaxial compressive strength
$\bar{f}_b$	Equibiaxial strength
G_f	Fracture energy
ε_p^{peak}	Plastic strain at peak under uniaxial compression
$\bar{f}_{c_0}$	Elastic limit stress under uniaxial compression

$$\bar{f}_t = \left(\frac{\bar{f}_c - 8 \text{ MPa}}{10 \text{ MPa}}\right)^{2/3} \times 1.40 \text{ MPa} \tag{A.1}$$

The equibiaxial compressive strength can be estimated as $\bar{f}_b = 1.16\bar{f}_c$ according to the experimental results reported by Kupfer et al. (1969).

Calibration of the present damage-plastic model consists in the determination of 15 parameters. These parameters are divided into four groups corresponding to the elastic properties, hardening, state at peak stress, and softening:

- The elastic properties are Young's modulus E and Poisson's ratio v.
- The hardening regime is defined by the initial value of the hardening variable q_{h_0} and the parameters of the hardening ductility measure A_h, B_h, C_h and D_h.
- The strength envelope in effective stress space is characterized by the values of uniaxial tensile strength $\bar{f}_t$, uniaxial compressive strength $\bar{f}_c$, and the eccentricity parameter e.
- The softening regime is defined by the control parameter ε_f of the damage law and the parameter A_s of the softening ductility measure.

Furthermore, both hardening and softening are affected by the parameters of the flow rule A_g and B_g.

A.2. Parameters of the strength envelope

The strength envelope (Menétrey–Willam failure surface) is defined by parameters $\bar{f}_c$, e and m_0. The compressive strength $\bar{f}_c$ is a material property and the eccentricity parameter e and friction parameter m_0 can be easily determined from the given strength values $\bar{f}_c$, $\bar{f}_t$ and $\bar{f}_b$.

The eccentricity parameter e that controls the shape of the deviatoric section can be evaluated using the formula given in Jirásek and Bažant (2002, p. 365):

$$e = \frac{1 + \epsilon}{2 - \epsilon}, \quad \text{where } \epsilon = \frac{\bar{f}_t}{\bar{f}_b} \frac{\bar{f}_b^2 - \bar{f}_c^2}{\bar{f}_c^2 - \bar{f}_t^2} \tag{A.2}$$

The friction parameter m_0 that controls the shape of the meridians can be determined as

$$m_0 = 3\frac{\bar{f}_c^2 - \bar{f}_t^2}{\bar{f}_c\bar{f}_t} \frac{e}{e + 1} \tag{A.3}$$

A.3. Parameters of the flow rule

Parameters A_g and B_g of the flow rule are calibrated using certain assumptions on the plastic flow in uniaxial tension and uniaxial compression. The flow rule (50) is split into a volumetric and a deviatoric part, i.e., the gradient of the plastic potential is decomposed as

$$\mathbf{m} = \frac{\partial g}{\partial \bar{\boldsymbol{\sigma}}} = \frac{\partial g}{\partial \bar{\sigma}_V} \frac{\partial \bar{\sigma}_V}{\partial \bar{\boldsymbol{\sigma}}} + \frac{\partial g}{\partial \bar{\rho}} \frac{\partial \bar{\rho}}{\partial \bar{\boldsymbol{\sigma}}} \tag{A.4}$$

Taking into account that $\partial \bar{\sigma}_V / \partial \bar{\boldsymbol{\sigma}} = \boldsymbol{\delta}/3$ and $\partial \bar{\rho}/\partial \bar{\boldsymbol{\sigma}} = \bar{\mathbf{s}}/\bar{\rho}$, restricting attention to the postpeak regime (in which $q_h = 1$) and differentiating the plastic potential (51), we rewrite Eq. (A.4) as

$$\mathbf{m} = \frac{\mathrm{d}m_g}{\mathrm{d}\bar{\sigma}_V} \frac{\boldsymbol{\delta}}{3\bar{f}_c} + \left(\frac{3}{\bar{f}_c} + \frac{m_0}{\sqrt{6}\bar{\rho}}\right) \frac{\bar{\mathbf{s}}}{\bar{f}_c} \tag{A.5}$$

Experimental results for concrete loaded in uniaxial tension indicate that the strains perpendicular to the loading direction are elastic in the softening regime. Thus, the plastic strain rate in these directions should be equal to zero ($m_2 = m_3 = 0$). Under uniaxial tension, the effective stress state at the end of hardening is characterized by $\bar{\sigma}_1 = \bar{f}_t$, $\bar{\sigma}_2 = \bar{\sigma}_3 = 0$, $\bar{\sigma}_V = \bar{f}_t/3$, $\bar{s}_1 = 2\bar{f}_t/3$, $\bar{s}_2 = \bar{s}_3 = -\bar{f}_t/3$ and $\bar{\rho} = \sqrt{2/3}\bar{f}_t$. Substituting this into (A.5) and enforcing the condition $m_2 = m_3 = 0$, we obtain an equation from which

$$\frac{\mathrm{d}m_\mathrm{g}}{\mathrm{d}\bar{\sigma}_\mathrm{V}}\bigg|_{\bar{\sigma}_\mathrm{V}=\bar{f}_\mathrm{t}/3} = \frac{3\bar{f}_\mathrm{t}}{\bar{f}_\mathrm{c}} + \frac{m_0}{2} \tag{A.6}$$

In uniaxial compressive experiments, a volumetric expansion is observed in the softening regime. Thus, the inelastic lateral strains are positive while the inelastic axial strain is negative. In the present approach, a constant ratio $D_\mathrm{f} = -m_2/m_1 = -m_3/m_1$ between lateral and axial plastic strain rates in the softening regime is assumed.

The effective stress state at the end of hardening under uniaxial compression is characterized by $\bar{\sigma}_1 = -\bar{f}_\mathrm{c}$, $\bar{\sigma}_2 = \bar{\sigma}_3 = 0$, $\bar{\sigma}_\mathrm{V} = -\bar{f}_\mathrm{c}/3$, $\bar{s}_1 = -2\bar{f}_\mathrm{c}/3$, $\bar{s}_2 = \bar{s}_3 = \bar{f}_\mathrm{c}/3$ and $\bar{\rho} = \sqrt{2/3}\bar{f}_\mathrm{c}$. Substituting this into (A.5) and enforcing the condition $m_2 = m_3 = -D_\mathrm{f}m_1$, we get an equation from which

$$\frac{\mathrm{d}m_\mathrm{g}}{\mathrm{d}\bar{\sigma}_\mathrm{V}}\bigg|_{\bar{\sigma}_\mathrm{V}=-\bar{f}_\mathrm{c}/3} = \frac{2D_\mathrm{f} - 1}{D_\mathrm{f} + 1}\left(3 + \frac{m_0}{2}\right) \tag{A.7}$$

Substituting the specific expression for $\mathrm{d}m_\mathrm{g}/\mathrm{d}\bar{\sigma}_\mathrm{V}$ constructed by differentiation of (52) into (A.6) and (A.7), we obtain two equations from which parameters

$$A_\mathrm{g} = \frac{3\bar{f}_\mathrm{t}}{\bar{f}_\mathrm{c}} + \frac{m_0}{2} \tag{A.8}$$

$$B_\mathrm{g} = \frac{\frac{1}{3}(1 + \bar{f}_\mathrm{t}/\bar{f}_\mathrm{c})}{\ln A_\mathrm{g} - \ln(2D_\mathrm{f} - 1) - \ln(3 + m_0/2) + \ln(D_\mathrm{f} + 1)} \tag{A.9}$$

can be computed.

The dependence of the gradient of the dilation parameter on the volumetric stress is shown in Fig. 17. The gradient of the dilation parameter, and therewith also the volumetric expansion, decreases with increasing confinement. The limit $\bar{\sigma}_\mathrm{V} \to -\infty$ corresponds to purely deviatoric flow. Good agreement with experimental results in uniaxial compression was found for $D_\mathrm{f} = 0.85$. This recommended value can be adjusted if the corresponding experimental results are available.

A.4. Hardening parameters

Parameter q_{h_0} is simply the dimensionless ratio $q_{\mathrm{h}_0} = \bar{f}_{\mathrm{c}_0}/\bar{f}_\mathrm{c}$.

Determination of parameters A_h, B_h, C_h and D_h that influence the hardening ductility measure is difficult. The effective stress varies within the hardening regime, even for monotonic loading, so that the ratio of axial and lateral plastic strain rate is not constant. Thus, an exact relation of all four model parameters to measurable material properties cannot be constructed. Comparison with experimental results (Section 4.1) has shown that a reasonable response is obtained with parameters $A_\mathrm{h} = 0.08$, $B_\mathrm{h} = 0.003$, $C_\mathrm{h} = 2$ and $D_\mathrm{h} = 1 \times 10^{-6}$.
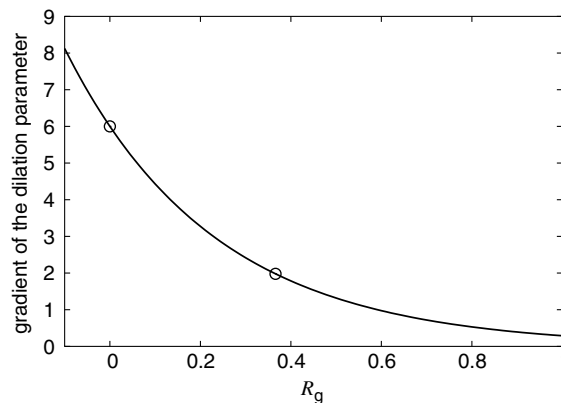

Fig. 17. The dependence of the gradient of the dilation parameter on R_g from Eq. (52). The values corresponding to uniaxial tension and uniaxial compression are marked.
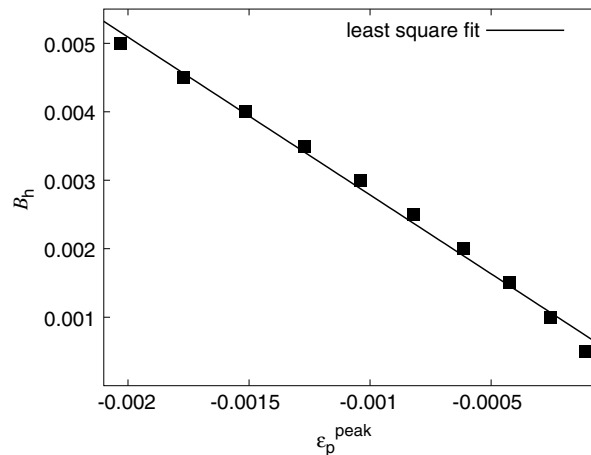
Fig. 18. The dependence of the parameter B_h on the axial plastic strain at peak under uniaxial compression.

However, the inelastic axial strain at peak may depend on the type of concrete and a modification of the values of these parameters is sometimes needed. The approach is based on the axial inelastic strain under uniaxial compression. Parameters A_h, C_h and D_h are set to their default values and only parameter B_h is varied. Furthermore, it is assumed that the calibration of the parameters of the flow rule has been done with $D_f = 0.85$. The relation between parameter B_h and the axial plastic strain at peak under uniaxial compression, ε_p^{peak}, is almost linear (see Fig. 18) and can be approximated by the linear expression

$$B_h = -2.29\varepsilon_p^{peak} + 0.00046 \qquad (A.10)$$

The influence of parameter B_h on the axial plastic strain at peak under uniaxial tension and under confined compression with a lateral confinement of 10 MPa is shown in Fig. 19. With increasing B_h, the plastic strain at peak in all three stress states increases. The influence in the uniaxial tension case is strongly nonlinear. Nevertheless, these plastic strains are still very small compared to the elastic strains at peak in uniaxial tension.

The dilation parameter D_f has a strong influence on the axial plastic strain at peak and, therewith, on the parameters of the ductility measure.

A.5. Summary of the calibration procedure

The eccentricity parameter e is determined from (A.2).

Parameters $A_h = 0.08$, $C_h = 2$ and $D_h = 1 \times 10^{-6}$ are taken by their default values, parameter B_h is evaluated from (A.10) or taken as $B_h = 0.003$.

Parameter m_0 is determined from (A.3) and used in evaluation of A_g and B_g according to (A.8) and (A.9).

Parameters ε_f and A_s are determined from the fracture energy G_f and from the softening part of the stress–strain curve under uniaxial compression. For localized failure modes, this curve should be adjusted according
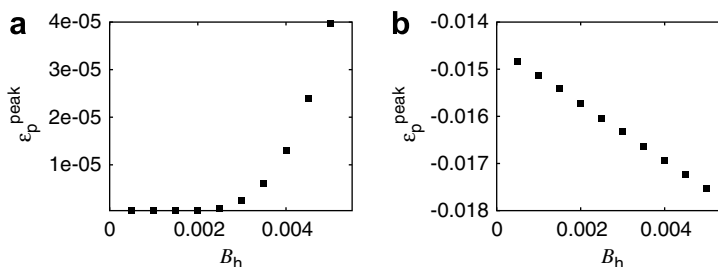

Fig. 19. The influence of the parameter B_h on the axial plastic strain at peak under (a) uniaxial tension and (b) triaxial compression.

to the element size. The recommended value of parameter A_s in the absence of sufficient experimental data is $A_s = 15$. For uniaxial tension, the hardening parameter is the axial plastic strain, since x_s from Eq. (62) is 1. Thus, (64) leads to an exponential curve of uniaxial tensile stress versus axial plastic strain.

It should be emphasized that the default values of various parameters should not be seen as universal constants, but only as first estimates when the available experimental results do not suffice to determine them.

Appendix B. Algorithmic stiffness

The algorithmic stiffness can be obtained by consistent differentiation of the stress-return algorithm with respect to the strain increment. We consider an incremental step from initial strain $\boldsymbol{\varepsilon}^{(n)}$ to final strain $\boldsymbol{\varepsilon} = \boldsymbol{\varepsilon}^{(n)} + \Delta\boldsymbol{\varepsilon}$, for which the stress-return algorithm provides the final effective stress $\bar{\boldsymbol{\sigma}}$. If the strain increment is changed by $\delta\boldsymbol{\varepsilon}$, the step from $\boldsymbol{\varepsilon}^{(n)}$ to $\boldsymbol{\varepsilon}^{(n)} + \Delta\boldsymbol{\varepsilon} + \delta\boldsymbol{\varepsilon}$ leads to final stress $\bar{\boldsymbol{\sigma}} + \delta\bar{\boldsymbol{\sigma}}$. Our goal is to find the dependence of $\delta\bar{\boldsymbol{\sigma}}$ on $\delta\boldsymbol{\varepsilon}$, provided that $\delta\boldsymbol{\varepsilon}$ is infinitesimal but $\Delta\boldsymbol{\varepsilon}$ is finite.

Since $\bar{\boldsymbol{\sigma}}$ is the result of the stress-return algorithm, it is given by (81) with principal effective stresses $\bar{\sigma}_I$ computed from (80), in which θ^{tr} is the Lode angle corresponding to the trial stress state and $\bar{\sigma}_V$ and $\bar{\rho}$ are obtained by solving Eqs. (75) and (77)–(79). All these relations must be consistently linearized. If the stress-return algorithm is run for the strain increment $\Delta\boldsymbol{\varepsilon} + \delta\boldsymbol{\varepsilon}$ instead of $\Delta\boldsymbol{\varepsilon}$, already the trial state will be different and in general the principal directions of the trial stress will change. Therefore, differentiation of (81) leads to

$$\delta\bar{\boldsymbol{\sigma}} = \sum_{I=1}^{3} \delta\bar{\sigma}_I \mathbf{n}_I \otimes \mathbf{n}_I + \sum_{I=1}^{3} \bar{\sigma}_I (\delta\mathbf{n}_I \otimes \mathbf{n}_I + \mathbf{n}_I \otimes \delta\mathbf{n}_I) \tag{B.1}$$

where $\delta\bar{\sigma}_I$ are the (infinitesimal) changes of principal effective stresses and $\delta\mathbf{n}_I$ are the (infinitesimal) changes of principal directions of the trial effective stress.

Due to elastic isotropy, principal directions of the trial effective stress $\delta\mathbf{n}_I$ coincide with the principal directions of the trial elastic strain, i.e., of $\boldsymbol{\varepsilon}_e^{\mathrm{tr}} = \boldsymbol{\varepsilon}^{(n)} - \boldsymbol{\varepsilon}_p^{(n)} + \Delta\boldsymbol{\varepsilon}$. Their changes caused by an infinitesimal change of $\Delta\boldsymbol{\varepsilon}$ denoted as $\delta\boldsymbol{\varepsilon}$ can be evaluated using general formulae for the dependence of normalized eigenvectors of a 3×3 matrix on the matrix itself, linearized about the current state. The procedure is formally the same as in Appendix I of Jirásek and Zimmermann (1998), and the resulting expression for the change of the first eigenvector reads

$$\delta\mathbf{n}_1 = \frac{\delta\varepsilon_{12}}{\varepsilon_{e1}^{\mathrm{tr}} - \varepsilon_{e2}^{\mathrm{tr}}} \mathbf{n}_2 + \frac{\delta\varepsilon_{13}}{\varepsilon_{e1}^{\mathrm{tr}} - \varepsilon_{e3}^{\mathrm{tr}}} \mathbf{n}_3 \tag{B.2}$$

where $\varepsilon_{eI}^{\mathrm{tr}}$ are the eigenvalues of $\boldsymbol{\varepsilon}_e^{\mathrm{tr}}$, and $\delta\varepsilon_{IJ} = \mathbf{n}_I \cdot \delta\boldsymbol{\varepsilon} \cdot \mathbf{n}_J$ are the components of $\delta\boldsymbol{\varepsilon}$ with respect to the coordinate system determined by unit vectors $\mathbf{n}_I, I = 1, 2, 3$. Similar expressions for changes of the second and third eigenvector follow from cyclic permutation of the subscripts. Combining (B.1) and (B.2), we can obtain convenient expressions for the changes of final stress components with respect to the coordinate system determined by fixed base vectors $\mathbf{n}_I$:

$$\delta\bar{\sigma}_{11} = \mathbf{n}_1 \cdot \bar{\boldsymbol{\sigma}} \cdot \mathbf{n}_1 = \delta\bar{\sigma}_1 \tag{B.3}$$

$$\delta\bar{\sigma}_{12} = \mathbf{n}_1 \cdot \bar{\boldsymbol{\sigma}} \cdot \mathbf{n}_2 = \frac{\bar{\sigma}_1 - \bar{\sigma}_2}{\varepsilon_{e1}^{\mathrm{tr}} - \varepsilon_{e2}^{\mathrm{tr}}} \delta\varepsilon_{12} \tag{B.4}$$

All the other components of $\delta\bar{\boldsymbol{\sigma}}$ follow again from cyclic permutation of subscripts. The change of the normal stress component $\delta\bar{\sigma}_{11}$ is equal to the change of the principal stress $\delta\bar{\sigma}_1$, which still needs to be analyzed. Before doing that, let us look at the change of the shear stress component $\delta\bar{\sigma}_{12}$, which is proportional to the change of the shear strain component $\delta\varepsilon_{12}$. The proportionality factor

$$2G_{12} = \frac{\bar{\sigma}_1 - \bar{\sigma}_2}{\varepsilon_{e1}^{\mathrm{tr}} - \varepsilon_{e2}^{\mathrm{tr}}} \tag{B.5}$$

seems to be undefined if the first two principal values of the trial elastic strain coincide, which happens e.g. under uniaxial compression. Fortunately, the expression for the shear stiffness G_{12} can be converted to a for-

mula that is applicable even in the case of multiple eigenvalues. Note that the principal effective stresses are given by (80) and their difference is

$$\bar{\sigma}_1 - \bar{\sigma}_2 = \sqrt{\frac{2}{3}} \bar{\rho} [\cos \theta^{\mathrm{tr}} - \cos(\theta^{\mathrm{tr}} - 2\pi/3)] \tag{B.6}$$

The principal values $\varepsilon_{eI}^{\mathrm{tr}}$ can be expressed in a form similar to (80), with $\bar{\sigma}_{\mathrm{V}}$, $\bar{\rho}$ and θ^{tr} replaced by the corresponding invariants of $\boldsymbol{\varepsilon}_{\mathrm{e}}^{\mathrm{tr}}$. The important point is that the Lode angle θ^{tr} remains the same, and so we can write

$$\varepsilon_{\mathrm{e}1}^{\mathrm{tr}} - \varepsilon_{\mathrm{e}2}^{\mathrm{tr}} = \sqrt{\frac{2}{3}} \rho_{\mathrm{e}}^{\mathrm{tr}} [\cos \theta^{\mathrm{tr}} - \cos(\theta^{\mathrm{tr}} - 2\pi/3)] \tag{B.7}$$

where $\rho_{\mathrm{e}}^{\mathrm{tr}} = \|\mathbf{e}_{\mathrm{e}}^{\mathrm{tr}}\|$ is the norm of the deviatoric part of $\boldsymbol{\varepsilon}_{\mathrm{e}}^{\mathrm{tr}}$. Substituting (B.6) and (B.7) into (B.5), we get $2G_{12} = \bar{\rho}/\rho_{\mathrm{e}}^{\mathrm{tr}}$. So the shear stiffness is well defined even if two principal stresses coincide. Only if all three principal stresses are equal, we need to make special provisions, because then $\bar{\rho} = 0$ and $\rho_{\mathrm{e}}^{\mathrm{tr}} = 0$. This is not surprising, since this case corresponds to a hydrostatic state (more specifically hydrostatic tension) and the stress returns to the vertex of the yield surface.

Now we turn attention to (B.3) and establish the link between the change of principal stress $\delta\bar{\sigma}_1$ and the change of strain $\delta\boldsymbol{\varepsilon}$. Differentiating the first equation from (80), we get

$$\delta\bar{\sigma}_1 = \delta\bar{\sigma}_{\mathrm{V}} + \sqrt{\frac{2}{3}} \cos \theta^{\mathrm{tr}} \delta\bar{\rho} - \sqrt{\frac{2}{3}} \bar{\rho} \sin \theta^{\mathrm{tr}} \delta\theta^{\mathrm{tr}} \tag{B.8}$$

The change of the Lode angle $\delta\theta^{\mathrm{tr}}$ can be evaluated directly from the definition of θ^{tr}. The Lode angle was defined in Eq. (43), based on the stress invariants. However, θ^{tr} is the Lode angle of the trial state and can be evaluated from the deviatoric invariants $J_{\mathrm{e}2}$ and $J_{\mathrm{e}3}$ of the trial elastic strain. Differentiation of the definition of Lode angle and of deviatoric invariants yields

$$\delta\theta^{\mathrm{tr}} = \frac{\sqrt{3}}{2 J_{\mathrm{e}2}^3 \sin 3\theta^{\mathrm{tr}}} \left(\frac{3}{2} \sqrt{J_{\mathrm{e}2}} J_{\mathrm{e}3} \delta J_{\mathrm{e}2} - J_{\mathrm{e}2}^{3/2} \delta J_{\mathrm{e}3} \right) = \frac{\sqrt{3}}{2 J_{\mathrm{e}2}^{5/2} \sin 3\theta^{\mathrm{tr}}} \left(\frac{3}{2} J_{\mathrm{e}3} \mathbf{e}_{\mathrm{e}}^{\mathrm{tr}} - J_{\mathrm{e}2} \mathbf{e}_{\mathrm{e}}^{\mathrm{tr}} \cdot \mathbf{e}_{\mathrm{e}}^{\mathrm{tr}} \right) : \delta\mathbf{e} \tag{B.9}$$

where $\mathbf{e}_{\mathrm{e}}^{\mathrm{tr}}$ is the deviatoric part of the trial elastic strain, $J_{\mathrm{e}2}$ and $J_{\mathrm{e}3}$ are its invariants, and $\delta\mathbf{e}$ is the deviatoric part of the strain change.

It remains to express the changes of effective stress invariants $\delta\bar{\sigma}_{\mathrm{V}}$ and $\delta\bar{\rho}$ that need to be substituted into (B.8) along with $\delta\theta^{\mathrm{tr}}$ from (B.9). Recall that the values of $\bar{\sigma}_{\mathrm{V}}$ and $\bar{\rho}$ are obtained by solving the set of four nonlinear equations (78), (79), (75) and (77). Linearization of these equations around their solution (that has been obtained by the stress-return algorithm) leads to a linear set of equations

$$\begin{bmatrix} 1 + K\Delta\lambda\dfrac{\partial m_{\mathrm{V}}}{\partial\bar{\sigma}_{\mathrm{V}}} & K\Delta\lambda\dfrac{\partial m_{\mathrm{V}}}{\partial\bar{\rho}} & K\Delta\lambda\dfrac{\partial m_{\mathrm{V}}}{\partial\kappa_{\mathrm{p}}} & Km_{\mathrm{V}} \\[2mm] 2G\Delta\lambda\dfrac{\partial m_{\mathrm{D}}}{\partial\bar{\sigma}_{\mathrm{V}}} & 1 + 2G\Delta\lambda\dfrac{\partial m_{\mathrm{D}}}{\partial\bar{\rho}} & 2G\Delta\lambda\dfrac{\partial m_{\mathrm{D}}}{\partial\kappa_{\mathrm{p}}} & 2Gm_{\mathrm{D}} \\[2mm] -\Delta\lambda\dfrac{\partial k_{\mathrm{p}}}{\partial\bar{\sigma}_{\mathrm{V}}} & -\Delta\lambda\dfrac{\partial k_{\mathrm{p}}}{\partial\bar{\rho}} & 1 & -k_{\mathrm{p}} \\[2mm] \dfrac{\partial f_{\mathrm{p}}}{\partial\bar{\sigma}_{\mathrm{V}}} & \dfrac{\partial f_{\mathrm{p}}}{\partial\bar{\rho}} & \dfrac{\partial f_{\mathrm{p}}}{\partial\kappa_{\mathrm{p}}} & 0 \end{bmatrix} \left\{ \begin{array}{c} \delta\bar{\sigma}_{\mathrm{V}} \\ \delta\bar{\rho} \\ \delta\kappa_{\mathrm{p}} \\ \delta\lambda \end{array} \right\} = \left\{ \begin{array}{c} \delta\bar{\sigma}_{\mathrm{V}}^{\mathrm{tr}} \\ \delta\bar{\rho}^{\mathrm{tr}} \\ 0 \\ -\dfrac{\partial f_{\mathrm{p}}}{\partial\theta}\delta\theta^{\mathrm{tr}} \end{array} \right\} \tag{B.10}$$

from which the infinitesimal changes $\delta\bar{\sigma}_{\mathrm{V}}$, $\delta\bar{\rho}$, $\delta\kappa_{\mathrm{p}}$ and $\delta\lambda$ can be calculated as linear combinations of the changes

$$\delta\bar{\sigma}_{\mathrm{V}}^{\mathrm{tr}} = K\boldsymbol{\delta} : \delta\boldsymbol{\varepsilon} \tag{B.11}$$

$$\delta\bar{\rho}^{\mathrm{tr}} = \frac{2G}{\bar{\rho}^{\mathrm{tr}}} \mathbf{s}^{\mathrm{tr}} : \delta\mathbf{e} \tag{B.12}$$

and of $\delta\theta^{\mathrm{tr}}$, which is given by (B.9).

The derived equations (B.3), (B.4) and (B.8)–(B.12) provide the relation between the infinitesimal changes of the strain increment and of the resulting effective stress provided by the stress-return algorithm. This relation is linear and can be symbolically written as $\delta\bar{\boldsymbol{\sigma}} = \mathbf{D}_{\mathrm{ep}}^{\mathrm{alg}} : \delta\boldsymbol{\varepsilon}$, where $\mathbf{D}_{\mathrm{ep}}^{\mathrm{alg}}$ is the elastoplastic algorithmic stiffness tensor. To get the overall algorithmic stiffness $\mathbf{D}^{\mathrm{alg}}$, we need to take into account the influence of damage.

The change of nominal stress

$$\delta\boldsymbol{\sigma} = (1 - \omega)\delta\bar{\boldsymbol{\sigma}} - \bar{\boldsymbol{\sigma}}\,\delta\omega \tag{B.13}$$

follows from the linearized form of (83). If the internal variable κ_{p} is below 1, damage vanishes, the effective stress is equal to the nominal one, and $\mathbf{D}^{\mathrm{alg}} = \mathbf{D}_{\mathrm{ep}}^{\mathrm{alg}}$. For larger values of κ_{p}, we express the change of damage by combining the linearized forms of (64) and (82):

$$\delta\omega = g_{\mathrm{d}}'\,\delta\tilde{\varepsilon} = \frac{g_{\mathrm{d}}'}{x_{\mathrm{s}}}\left[\Delta\lambda\left(\frac{\partial m_{\mathrm{V}}}{\partial\bar{\sigma}_{\mathrm{V}}} - \frac{m_{\mathrm{V}}x_{\mathrm{s}}'}{x_{\mathrm{s}}}\right)\delta\bar{\sigma}_{\mathrm{V}} + \Delta\lambda\frac{\partial m_{\mathrm{V}}}{\partial\bar{\rho}}\delta\bar{\rho} + \Delta\lambda\frac{\partial m_{\mathrm{V}}}{\partial\kappa_{\mathrm{p}}}\delta\kappa_{\mathrm{p}} + m_{\mathrm{V}}\,\delta\lambda\right] \tag{B.14}$$

where $g_{\mathrm{d}}' = \mathrm{d}g_{\mathrm{d}}/\mathrm{d}\kappa_{\mathrm{d}}$ and $x_{\mathrm{s}}' = \mathrm{d}x_{\mathrm{s}}/\mathrm{d}\bar{\sigma}_{\mathrm{V}}$ are the derivatives of the functions defined in (64) and (62). The changes $\delta\bar{\sigma}_{\mathrm{V}}$, $\delta\bar{\rho}$, $\delta\kappa_{\mathrm{p}}$ and $\delta\lambda$ can be expressed in terms of $\delta\boldsymbol{\varepsilon}$ following the same procedure as for the plastic part of the model, i.e., based on Eqs. (B.9)–(B.12).

Appendix C. Analysis of plastic potential

In this appendix we prove the inequality that was exploited in Section 3.3 in the proof of thermodynamic admissibility of the present damage-plastic model. We need to show that for any stress state on the yield surface the value of the plastic potential is larger than that evaluated at the origin (i.e., at zero stress state) using the same value of the hardening variable. Mathematically speaking, we need to show that

$$g_{\mathrm{p}}(\bar{\sigma}_{\mathrm{V}}, \bar{\rho}; \kappa_{\mathrm{p}}) - g_{\mathrm{p}}(0, 0; \kappa_{\mathrm{p}}) \geqslant 0 \tag{C.1}$$

whenever there exists $\bar{\theta} \in \langle 0, \pi/3\rangle$ such that

$$f_{\mathrm{p}}(\bar{\sigma}_{\mathrm{V}}, \bar{\rho}, \bar{\theta}; \kappa_{\mathrm{p}}) = 0 \tag{C.2}$$

To simplify notation, we will introduce dimensionless stress variables $S = \bar{\sigma}_{\mathrm{V}}/\bar{f}_{\mathrm{c}}$ and $R = \bar{\rho}/\sqrt{6}\bar{f}_{\mathrm{c}}$ and a constant parameter $Q = A_{\mathrm{g}}B_{\mathrm{g}}\exp(-\bar{f}_{\mathrm{t}}/3B_{\mathrm{g}}\bar{f}_{\mathrm{c}})$. Comparing the yield function (47) and the plastic potential (51), we realize that the first term in curly brackets is in both expressions the same. Consequently, subtracting the left-hand side of (C.2) from the left-hand side of (C.1) and taking into account that q_{h}^2 is always positive, we obtain an equivalent yet simpler condition

$$1 - m_0(r - 1)R - m_0 S + Q\left(\exp\frac{S}{B_{\mathrm{g}}} - 1\right) \geqslant 0 \tag{C.3}$$

It is sufficient to show that this inequality is satisfied for all stress states inside the limit failure envelope, i.e., for all values of R and S for which

$$9R^2 + m_0(rR + S) - 1 \leqslant 0 \tag{C.4}$$

In the above, parameter r can attain values between 1 and $1/e$ where e is the eccentricity parameter, typically slightly larger than 0.5. Note that the dimensionless stress R is always nonnegative while S can have any sign but cannot exceed $1/m_0$.

The proof is facilitated if we treat separately the cases of positive and negative volumetric stress. Firstly, for $S \geqslant 0$ we have $\exp(S/B_{\mathrm{g}}) \geqslant 1$ and it is sufficient to show that $1 - m_0(r - 1)R - m_0 S \geqslant 0$, which easily follows from (C.4). Secondly, for $S \leqslant 0$ we can minimize the expression on the left-hand side of (C.3) with respect to R by substituting the maximum possible value of R that satisfies (C.4), namely $R = [\sqrt{m_0^2 r^2 + 36(1 - m_0 S)} - m_0 r]/18$. In this way we obtain a sufficient condition in terms of S and r only,

$$F(S, r) \equiv 1 - \frac{m_0(r - 1)}{18}\left[\sqrt{m_0^2 r^2 + 36(1 - m_0 S)} - m_0 r\right] - m_0 S + Q\left(\exp\frac{S}{B_{\mathrm{g}}} - 1\right) \geqslant 0 \tag{C.5}$$
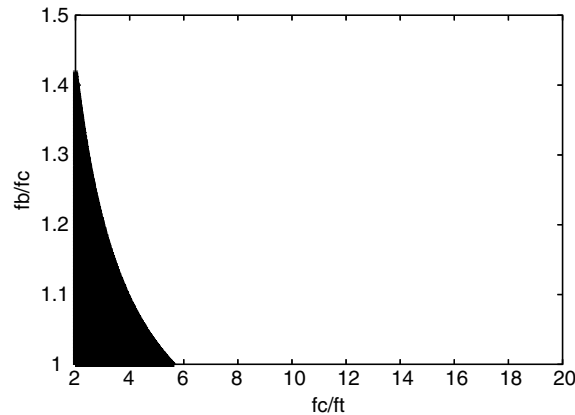
Fig. 20. Combinations of strength ratios leading to thermodynamically admissible model (blank region).

Furthermore, it is possible to show that function F defined in (C.5) is for any fixed $S \leqslant 0$ a decreasing function of $r \geqslant 1$ and thus attains its minimum for the maximum possible value of r, i.e., for $r = 1/e$. Finally, for fixed $r = 1/e$, $F(S, 1/e)$ is a convex function of S and condition (C.5) is certainly satisfied for all $S \leqslant 0$ if

$$F(0, 1/e) = 1 - \frac{m_0(1-e)}{18} \left(\sqrt{m_0^2 + 36e^2} - m_0 \right) \geqslant 0 \tag{C.6}$$

$$\frac{\partial F(0, 1/e)}{\partial S} = \frac{m_0^2(1-e)}{\sqrt{m_0^2 + 36e^2}} - m_0 + \frac{Q}{B_g} \leqslant 0 \tag{C.7}$$

The first of these conditions is satisfied for all $m_0 > 0$ and $0 < e < 1$, as can be verified by simple algebraic manipulations. The second condition can be transformed to

$$\frac{1-e}{\sqrt{1 + \left(\frac{6e}{m_0} \right)^2}} + \frac{A_g}{m_0} \exp \left(-\frac{\bar{f}_t}{3\bar{f}_c B_g} \right) \leqslant 1 \tag{C.8}$$

Whether this is true depends on the specific values of model parameters $\bar{f}_t$, $\bar{f}_c$, e, m_0, A_g and B_g. If the parameters are determined using the procedure described in Appendix A, the value of the left-hand side of (C.8) depends only on the dimensionless strength ratios $\gamma = \bar{f}_c / \bar{f}_t$ and $\beta = \bar{f}_b / \bar{f}_c$. For example, for $\gamma = 10$ and $\beta = 1.16$ we obtain $e = 0.5229$, $m_0 = 10.198$, $A_g = 5.399$ and $B_g = 0.6474$, and the value of the left-hand side is 0.9588, i.e., the condition is satisfied. The shaded area in Fig. 20 corresponds to the combinations of strength ratios γ and β for which condition (C.8) is violated. It is clear that the condition is satisfied for all practically relevant cases. It is for instance sufficient if $\bar{f}_b \geqslant \bar{f}_c$ and $\bar{f}_c \geqslant 6\bar{f}_t$. This concludes the proof of thermodynamic consistency of the model.

References

Ananiev, S., Ožbolt, J., 2004. Plastic-damage model for concrete in principal directions. In: Li, V., Leung, C.K.Y., Willam, K.J., Billington, S.L. (Eds.), Fracture Mechanics of Concrete Structures, pp. 271–278.

Bažant, Z.P., Oh, B.-H., 1983. Crack band theory for fracture of concrete. Materials and Structures 16, 155–177.

Bažant, Z.P., Adley, M.D., Carol, I., Jirásek, M., Akers, S.A., Rohani, B., Cargile, J.D., Caner, F.C., 2000. Large-strain generalization of microplane model for concrete and applications. Journal of Engineering Mechanics, ASCE 126, 971–980.

Bleich, F., 1952. Buckling Strength of Metal Structures. McGraw-Hill, New York.

Bourgeois, F., Burlion, N., Duveau, G., Shao, J.-F., 2003. Mise en oeuvre d'une modélisation élasto-plastique endommageable du béton. Revue Française de Génie Civil 7, 583–594.

Caner, F.C., Bažant, Z.P., 2000. Microplane model M4 for concrete. II. Algorithm and calibration. Journal of Engineering Mechanics, ASCE 126, 954–961.

Caner, F.C., Bažant, Z.P., Červenka, J., 2002. Vertex effect in strain-softening concrete at rotating principal axes. Journal of Engineering Mechanics, ASCE 128, 24–33.

Carol, I., Rizzi, E., Willam, K.J., 2001. On the formulation of anisotropic elastics degradation. II. Generalized pseudo-Rankine model for tensile damage. International Journal of Solids and Structures 38, 519–546.

CEB-FIP Model Code 1990, Design Code, 1991. Thomas Telford, London.

Červenka, J., Červenka, V., Eligehausen, R., 1998. Fracture-plastic material model for concrete, application to analysis of powder actuated anchors. In: Mihashi, H., Rokugo, K. (Eds.), Fracture Mechanics of Concrete Structures. Aedificatio Publishers, Freiburg, Germany, pp. 1107–1117.

Chen, A.C., Chen, W.F., 1975. Constitutive relations for concrete. Journal of Engineering Mechanics Division, ASCE 101, 465–481.

Contrafatto, L., Cuomo, M., 2002. A new thermodynamically consistent continuum model for hardening plasticity coupled with damage. International Journal of Solids and Structures 39, 6241–6271.

Cottle, R.W., Pang, J.-S., Stone, R.E., 1992. The Linear Complementarity Problem. Academic Press, Boston.

Dragon, A., Mróz, Z., 1979. A continuum model for plastic-brittle behavior of rock and concrete. International Journal of Engineering Science 17, 121–137.

Etse, G., Willam, K.J., 1994. A fracture-energy based constitutive formulation for inelastic behavior of plain concrete. Journal of Engineering Mechanics, ASCE 120, 1983–2011.

Feenstra, P.H., de Borst, R., 1996. A composite plasticity model for concrete. International Journal of Solids and Structures 33, 707–730.

Gatuingt, F., Pijaudier-Cabot, G., 2002. Coupled damage and plasticity modelling in transient dynamic analysis of concrete. International Journal of Numerical and Analytical Methods in Geomechanics 26, 1–24.

Gerard, G., Becker, H., 1957. Handbook of structural stability. Part I, buckling of flat plates. Technical Note 3781, National Advisory Committee for Aeronautics.

Gopalaratnam, V.S., Shah, S.P., 1985. Softening response of plain concrete in direct tension. Journal of the American Concrete Institute 82, 310–323.

Grassl, P., 2004. Modelling of dilation of concrete and its effect in triaxial compression. Finite Elements in Analysis and Design 40, 1021–1033.

Grassl, P., Jirásek, M., 2006. Plastic model with non-local damage applied to concrete. International Journal of Numerical and Analytical Methods in Geomechanics 30, 71–90.

Grassl, P., Lundgren, K., 2003. Localisation of deformations in concrete subjected to compression. In: Proceedings of Euro-C. Balkema, Rotterdam.

Grassl, P., Lundgren, K., Gylltoft, K., 2002. Concrete in compression: a plasticity theory with a novel hardening law. International Journal of Solids and Structures 39, 5205–5223.

Hansen, E., Willam, K., Carol, I., 2001. A two-surface anisotropic damage/plasticity model for plain concrete. In: de Borst, R., Mazars, J., Pijaudier-Cabot, G., van Mier, J.G.M. (Eds.), Fracture Mechanics of Concrete Structures. Balkema, Lisse, pp. 549–556.

Imran, I., Pantazopoulou, S.J., 1996. Experimental study of plain concrete under triaxial stress. ACI Materials Journal 93, 589–601.

Imran, I., Pantazopoulou, S.J., 2001. Plasticity model for concrete under triaxial compression. Journal of Engineering Mechanics, ASCE 127, 281–290.

Jason, L., Pijaudier-Cabot, G., Huerta, A., Crouch, R., Ghavamian, S., 2004. An elastic plastic damage formulation for the behavior of concrete. In: Li, V., Leung, C.K.Y., Willam, K.J., Billington, S.L. (Eds.), Fracture Mechanics of Concrete Structures, pp. 549–556.

Jason, L., Huerta, A., Pijaudier-Cabot, G., Ghavamian, S., in press. An elastic plastic damage formulation for concrete: application to elementary and structural tests. Computer Methods in Applied Mechanics and Engineering.

Jirásek, M., Bažant, Z.P., 2002. Inelastic Analysis of Structures. John Wiley and Sons, Chichester.

Jirásek, M., Zimmermann, T., 1998. Analysis of rotating crack model. Journal of Engineering Mechanics, ASCE 124, 842–851.

Ju, J.W., 1989. On energy-based coupled elastoplastic damage theories: constitutive modeling and computational aspects. International Journal of Solids and Structures 25 (7), 803–833.

Kang, H.D., 1997. Triaxial Constitutive Model for Plain and Reinforced Concrete Behavior. Ph.D. Thesis, University of Colorado, Boulder, CO.

Kang, H.D., Willam, K.J., 1999. Localization characteristics of triaxial concrete model. Journal of Engineering Mechanics, ASCE 125, 941–950.

Karsan, I.D., Jirsa, J.O., 1969. Behavior of concrete under compressive loadings. Journal of the Structural Division, ASCE 95, 2543–2563.

Krätzig, W., Polling, R., 2004. An elasto-plastic damage model for reinforced concrete with minimum number of material parameters. Computers and Structures 82, 1201–1215.

Kupfer, H., Hilsdorf, H.K., Rüsch, H., 1969. Behavior of concrete under biaxial stresses. Journal of the American Concrete Institute 66, 656–666.

Lade, P.V., Kim, M.K., 1995. Single hardening constitutive model for soil, rock and concrete. International Journal of Solids and Structures 32, 1963–1978.

Lee, J., Fenves, G.L., 1998. Plastic-damage model for cyclic loading of concrete structures. Journal of Engineering Mechanics, ASCE 124, 892–900.

Lin, F.-B., Bažant, Z.P., Chern, J.-C., Marchertas, A.H., 1987. Concrete model with normality and sequential identification. Computers and Structures 26, 1011–1025.

Lubliner, J., Oliver, J., Oller, S., Oñate, E., 1989. A plastic-damage model for concrete. International Journal of Solids and Structures 25 (3), 299–326.

Markeset, G., Hilleborg, A., 1995. Softening of concrete in compression – localization and size effects. Cement and Concrete Research 25 (4), 702–708.

Mazars, J., 1984. Application de la mécanique de l'endommagement au comportement non linéaire et à la rupture du béton de structure. Thèse de Doctorat d'Etat, Université Paris VI, France.

Menétrey, P., Willam, K.J., 1995. A triaxial failure criterion for concrete and its generalization. ACI Structural Journal 92, 311–318.

Nemecek, J., Padevet, P., Patzak, B., Bittnar, Z., 2005. Effect of transversal reinforcement in normal and high strength concrete columns. Materials and Structures 38 (281), 665–671.

Pekau, O.A., Zhang, Z.X., 1994. Strain-space cracking model for concrete and its application. Computers and Structures 51, 151–162.

Pramono, E., Willam, K., 1989. Fracture energy-based plasticity formulation of plain concrete. Journal of Engineering Mechanics, ASCE 115, 1183–1203.

Salari, M.R., Saeb, S., Willam, K.J., Patchet, S.J., Carrasco, R.C., 2004. A coupled elastoplastic damage model for geomaterials. Computer Methods in Applied Mechanics and Engineering 193, 2625–2643.

Willam, K.J., Warnke, E.P., 1974. Constitutive model for the triaxial behavior of concrete. In: Concrete Structures Subjected to Triaxial Stresses. Vol. 19 of IABSE Report, International Association of Bridge and Structural Engineers, Zurich, May, pp. 1–30.